Progetto S3 – Scenari di scuotimento in aree di interesse prioritario e/o strategico

Responsabili: Francesca Pacor (INGV-MI) e Marco Mucciarelli (Unibas)

TASK 6 – GUBBIO - DELIVERABLE D20

BEDROCK SHAKING SCENARIOS

A cura di:
UR1 – *F. Pacor, G. Ameri, E. Fiorini, G. Franceschina*
UR2 – *G. Cultrera*
UR10 – *A. Emolo, F. Gallovic, V. Convertito, A. Zollo*
INGV-RM - *R. Basili*

July 2007

INDEX

1. INTRODUCTION

The main goal of Task 6 is the computation of the bedrock and site seismic scenarios in the Gubbio town and in the Gubbio basin (Central Italy). This area represents one of the prediction case studies, planned in the framework of Project S3 which aims at simulating ground shaking scenarios for moderate magnitude earthquakes.

Deterministic shaking scenarios, described in this report, are computed for the Maximum Credible Earthquake. This is associated with two sources capable of generating an earthquake with M equal to 6 and located at about 10km from the sites.

Starting from these sources bedrock shaking scenarios at different level of complexity are computed by ground motion prediction equations (scenarios of level 0), high frequency (f>0.5Hz) simulations (scenarios of level 1) and broad band (0-20 Hz) simulations (scenarios of level 2). However since many sites have to be simulated for accurately sampling the basin, the bedrock ground motions for evaluating the seismic response of the valley are generated at level 1.
For four test sites a comparison between time series computed at different levels of complexity have been performed in order to verify the approximations introduced in level 1.
Before computing the predicted shaking scenarios, we evaluate the modelling capability of the adopted simulation techniques reproducing the observed ground motions occurred during the 1984 Gubbio earthquake (M 5.7).
Finally we apply the probabilistic-deterministic approach for a characteristic earthquake scenario proposed by Convertito *et al.* (2006) to perform hazard analysis considering the two seismogenic faults at three sites of interest in the Gubbio area (paragraph 3.3). In this way, respect to the deterministic approach, we produce 'dynamic shaking scenarios' introducing the time variable.

The shaking scenarios generated in the Gubbio area allow us to show how the prediction of the ground motion can be tackled using different methodologies and which strategy should be followed to select mean shaking scenario. As the available information increases, we could gradually adopt approaches more and more sophisticated and provide shaking scenarios that account for specific effects related to the source and propagation (e.g., directivity, radiation pattern distribution,…). Furthermore, the adoption of different approaches allows a cross check of the results guaranteeing the reliability of the ground motion estimates.

2. DEFINITION OF REFERENCE EARTHQUAKES

2.1 TECTONIC SETTING AND SEISMICITY

The Gubbio basin lies in the middle of the northern Apennine mountain belt. This area is dominated by NW-SE striking, SW dipping Quaternary normal faults (Fig. 2.1.1).

Fig. 2.1.1 – Oblique view of peninsular Italy showing the main faulting types in wide regions and the Seismogenic Areas (composite faults) that appear in DISS v. 3.0.2.

Although in the Apennines the identification of earthquakes causative faults is not straightforward, a good agreement exists between the long-term kinematics of Quaternary faults and focal mechanisms of recent major earthquakes (Barba and Basili, 2000).
Most of these normal faults apparently die at depth against the so called Etrurian Fault System (EFS; Boncio et al., 2000), an East-dipping low-angle major normal fault system stretching from northern Tuscany to southern Umbria. To the West of the EFS, the crust becomes progressively thinner and hotter and tectonics is dominated by volcanic or volcano-related processes. To the East, active normal faulting is found up until the Apennine main drainage divide. On the eastern flank of the Apennines, crustal and sub crustal active tectonics is dominated by West-dipping thrust faulting.

The area around Gubbio was affected by several moderate earthquakes in historical time. Table 2.1.1 shows a selection from the CPTI04 catalog (CPTI Working Group,

2004) of historical earthquakes within 25 km from Gubbio.

Table 2.1.1 – Selection from the CPTI04 catalog of the largest earthquakes within 25 km from Gubbio.

#	Yyyy/mm/dd	Area	Io	Lat	Lon	Mw
161	1465/05/17	GUBBIO	VI	43.351	12.577	4.83
162	1466/12/26	GUBBIO	VI	43.351	12.577	4.83
166	1471/03/	PICCIONE	VI	43.250	12.500	4.83
285	1593/04/23	GUBBIO	VII-VIII	43.271	12.676	5.50
291	1595/10/30	GUBBIO	V-VI	43.351	12.577	4.63
451	1712/03/28	FRONTONE	VII-VIII	43.513	12.734	5.30
535	1751/07/27	GUALDO TADINO	X	43.222	12.730	6.30
538	1752/07/14	PADULE	VI	43.333	12.667	4.83
1266	1897/03/01	CASA CASTALDA	VI-VII	43.167	12.600	5.03
1275	1897/06/24	PIANELLO	VI	43.533	12.567	4.83
1286	1897/12/18	APP. UMBRO-MARCHI.	VII	43.500	12.380	5.18
1563	1912/05/11	PIANELLO	V-VI	43.567	12.500	4.63
1586	1913/08/09	M.LETO	V-VI	43.400	12.500	4.63
1600	1914/07/31	GUALDO TADINO	VII	43.200	12.800	5.16
1715	1921/04/05	CASTIGLIONE	VI	43.300	12.500	4.83
1798	1927/11/30	M.LETO	VI	43.400	12.500	4.83
2159	1961/03/23	GUBBIO	VI-VII	43.362	12.544	4.37
2186	1963/02/03	PIETRALUNGA	VI	43.433	12.450	4.83
2190	1963/05/20	M.LETO	VI	43.400	12.500	4.83
2295	1971/02/11	CASA CASTALDA	VI	43.183	12.667	4.77
2308	1971/12/18	FOSSATO	V	43.317	12.750	4.51
2320	1973/04/19	COSTACCIARO	VI	43.400	12.800	4.75
2912	1982/10/17	VALFABBRICA	VI	43.164	12.647	4.61
2974	1984/04/29	GUBBIO/VALFABBRICA	VII	43.256	12.530	5.68
3728	2000/06/22	APP. UMBRO-MARCHI.	-	43.345	12.434	4.63

2.2 SEISMOGENIC SOURCES

The faults illustrated in this section are those that appear in DISS v. 3.0.2, a database of seismogenic sources for Italy and some surrounding countries (DISS Working Group, 2006; Basili et al., 2007).

In the Gubbio area, DISS shows two major sources (ITGG037, ITGG038), that were identified and characterized by Pucci et al. (2003) mainly by surface and subsurface geological investigations. Figure 2.2.1 and Table 2.2.1 show a map of the seismogenic sources and their parameters, respectively. The uncertainties associated to these parameters are based on geological wisdom, taking into account the accuracy of investigation methods and techniques.

The fault to the south (ITGG037) is thought to be the source of the 1984 Gubbio earthquake. The fault to the north (ITGG038) is a sibling structure of the ITGG037 but has not released any earthquake in historical time. This latter fault appears with similar geometry of the former in seismic lines and at the surface (Barchi et al., 2000), therefore it has similar parameters.

These faults would be able to generate a bigger earthquake than that actually occurred in 1984. This circumstance arises because Pucci et al. (2003) found geological evidence for a fault of a larger size.

Table 2.2.1 – Fault parameters.

ID	ITGG037	ITGG037mod*	ITGG038	Uncertainty
Lon Centroid	12.5682	12.5559	12.4667	±0.01
Lat Centroid	43.2251	43.2284	43.3012	±0.01
Strike (deg)	130	130	130	±10
Dip (deg)	20	20	20	±5
Rake (deg)	270	270	270	±10
Length (km)	10.0	8.0	10.0	±2
Width (km)	7.0	6.0	7.0	±2
Min Depth (km)	4.0	4.3	2.5	±1
Max Depth (km)	6.4	6.4	4.9	±2
Slip (m)	0.5	0.3	0.5	±0.1
M_0 (Nm)	1.05E+18	4.32E+17	1.05E+18	
Mw	6.0	5.7	6.0	

*Fault modified to fit the 1984 earthquake.

Fig. 2.2.1 – Map showing the seismogenic sources of the Gubbio area. In red the seismogenic sources as they appear in DISS; in blue the seismogenic source modified to better fit the 1984 seismic event.

In 1984, the ITGG037 fault apparently did not release its maximum allowable earthquake. For the purpose of this study, we propose the fault ITGG037mod, modified from the original database record with parameters that fit the size of the 1984 earthquake. It is worth notice that southeast of Gubbio, in the Gualdo Tadino area, an Mw 6.3 earthquake occurred in 1751 (Table 2.1.1). The magnitude of this event might actually be slightly smaller because it can be affected by an overestimation of damage due to the 1747 earthquake, located a few kilometers to the east. The source of the 1751 earthquake has not been positively identified and, as such, it does not appear, as yet, in the DISS database. The Gubbio faults, however, may be part of a longer system that extends to the southeast until it joins the Colfiorito Fault System. This hypothesis is also supported by geodetic and seismic data about the April 3, 1998, Mw 5.1 earthquake (De Martini et al., 2003; Ciaccio et al., 2005).

3. SHAKING SCENARIOS

3.1 PARAMETERS FOR SIMULATIONS

Hereinafter the parameters needed for performing the simulation studies in the Gubbio areas are given. The information provided includes the faults characteristics, the propagation medium properties, and the coordinates of the receivers to be used.

3.1.1 Faults characteristics

Two faults segments have been considered in the simulation study: ITGG037 and ITGG038 (Figure 3.1.1). The characteristics of both faults are from the DISS (2006) database. We have also considered a part of the ITGG037 (identified as ITGG037-mod) as the causative fault of the April 29, 1984, M5.7 Gubbio earthquake. The simulation of the 1984 Gubbio earthquake has been used for calibration purposes. The fault characteristics are reported in the Table 2.2.1.

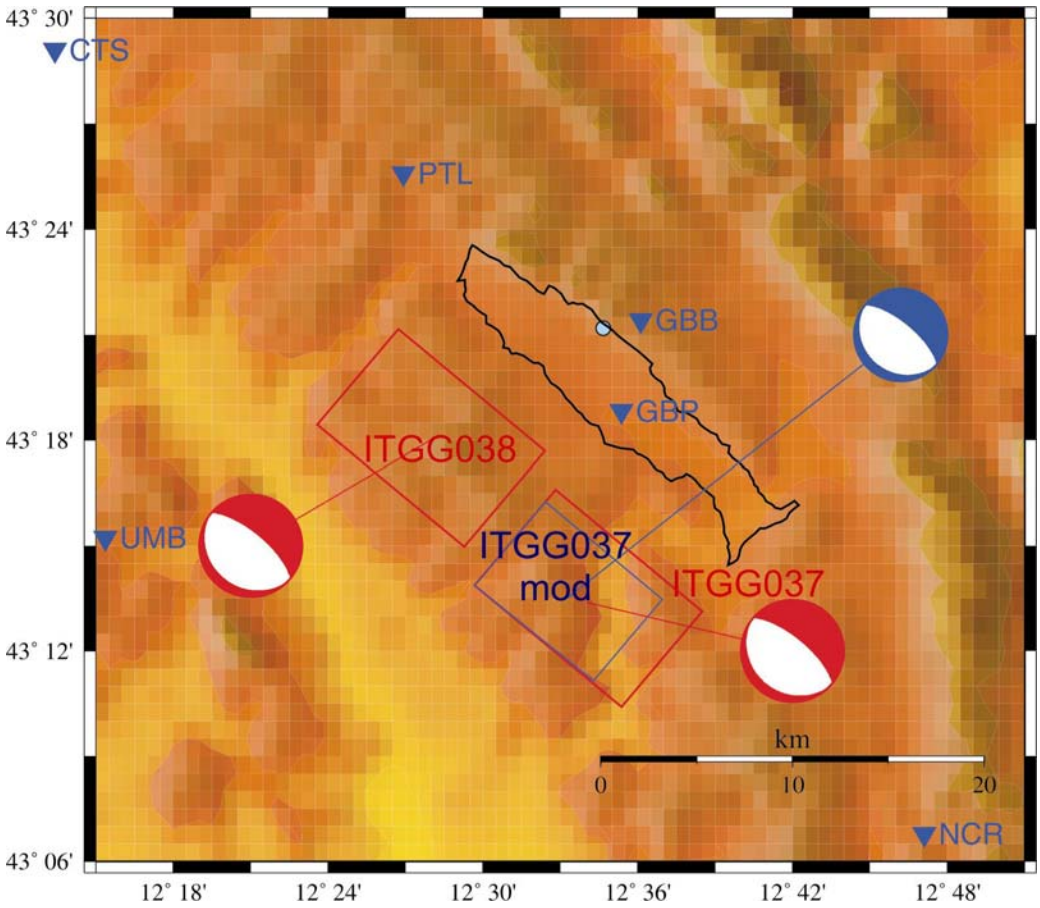

Figure 3.1.1 – Faults used in the simulation study. The fault plane solution are also shown. The black line identifies the limit of the Gubbio basin. The cyan circle represents Gubbio city (GCT station) while the inverted blue triangles are the accelerometric stations (CTS, Città di Castello; GBB, Gubbio; GBP, Gubbio Piana; NCR, Nocera Umbra; PTL, Pietralunga; UMB, Umbertide).

3.1.2. Crustal velocity model

The properties of the propagation medium are reported in the Table 3.1.1 and were provided by Moretti and De Gori (personal communication).

Table 3.1.1 – Crustal velocity model.

Depth in km	V_P in km/s	$V_S=V_P/1.88$ in km/s
0.0	4.05	2.17
1.0	4.62	2.47
2.0	5.19	2.76
3.0	5.86	3.10
5.0	6.20	3.33
6.0	6.40	3.48
12.0	6.50	3.53
24.0	6.60	3.59

The attenuation model was derived by Castro et al. (2004):

$$Q(f) = \begin{cases} 31.2\, f^{1.2} & for\ f < 9.0\ Hz \\ \\ 438 & for\ f > 9.0\ Hz \end{cases}$$

The *k*-decay should not be required due to the constant Q value at high frequencies.

3.1.3. Accelerometric stations

The accelerometric stations used in the simulation study are shown in the Figure 3.1.1 while their coordinates are reported in the Table 3.1.2. In the table is also included the Gubbio City station (GCT/GUB) that has been considered in the study.

Table 3.1.2 – Accelerometric station coordinates.

		Geographical coord.		
Station name	**Code**	**Lon.**	**Lat.**	**Site**
Gubbio	GBB	12.601944	43.356944	Rock
Gubbio Piana	GBP	12.589550	43.313816	Soft soil
Umbertide	UMB	12.256111	43.253889	Rock
Pietralunga	PTL	12.448611	43.426667	Rock
Nocera Umbra	NCR	12.785000	43.113000	Rock
Città di Castello	CTS	12.223611	43.485000	Soft soil
Gubbio City	GCT/GUB	12.5778	43.3531	Rock

3.1.4. Basin stations

Basin stations are shown in the Figure 3.1.2 and their coordinates are reported in the Table 3.1.3.

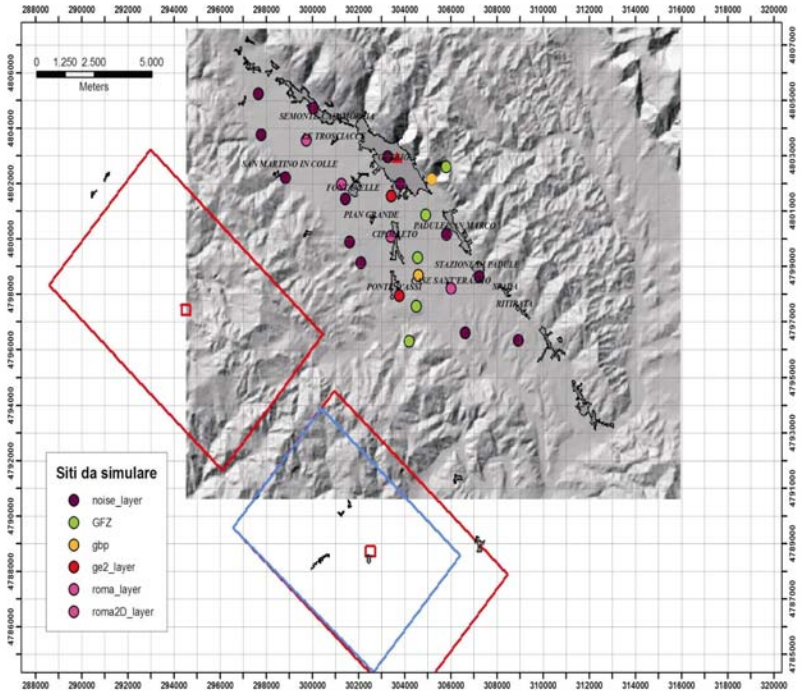

Figure 3.1.2 – Gubbio basin stations.

Table 3.1.4 – Basin station coordinates.

		Geographical coord.	
Owner	Code	Lon.	Lat.
GFZ	GU00	12.604	43.351
GFZ	GU03	12.593	43.335
GFZ	GU07	12.590	43.321
GFZ	GU09	12.589	43.306
GFZ	GU10	12.586	43.294
INGVrm	EU01	12.608	43.312
INGVrm	EU09	12.529	43.358
INGVrm	EU04	12.575	43.328
INGVrm	EU07	12.548	43.344
UNIGE	STAb	12.5763	43.3491
UNIGE	STAe	12.5795	43.3070
UNIGE	STAc	12.5740	43.3393
UNISI	15_PVit	12.5795	43.3444
UNISI	A1K	12.5595	43.3183
UNISI	A2K	12.5533	43.3248
UNISI	A3F	12.5182	43.3451
UNISI	A4K	12.5046	43.3587
UNISI	B9	12.5504	43.3389
UNISI	C04	12.5322	43.3681
UNISI	C09	12.5025	43.372
UNISI	C15	12.5725	43.353
UNISI	C23	12.6049	43.3285
UNISI	C27	12.623	43.315
UNISI	N14	12.6447	43.2948
UNISI	N17	12.6161	43.2966

3.2 THE 1984 GUBBIO EARTHQUAKE (M 5.7) SIMULATION

The April 29, 1984 (5:03 GMT) earthquake struck the Northern Umbria region with magnitude M 5.7. The municipalities with major damages were Assisi, Gubbio, Perugia, Città di Castello, Valfabbrica, Umbertide, Gualdo Tadino, and about 300.000 people were involved. Figure 3.2.1 shows the distribution of the felt intensity (MCS) ranging between V and VII in the epicentral area (INGV-Data Base Macrosismico italiano, DBMI04; 2007).

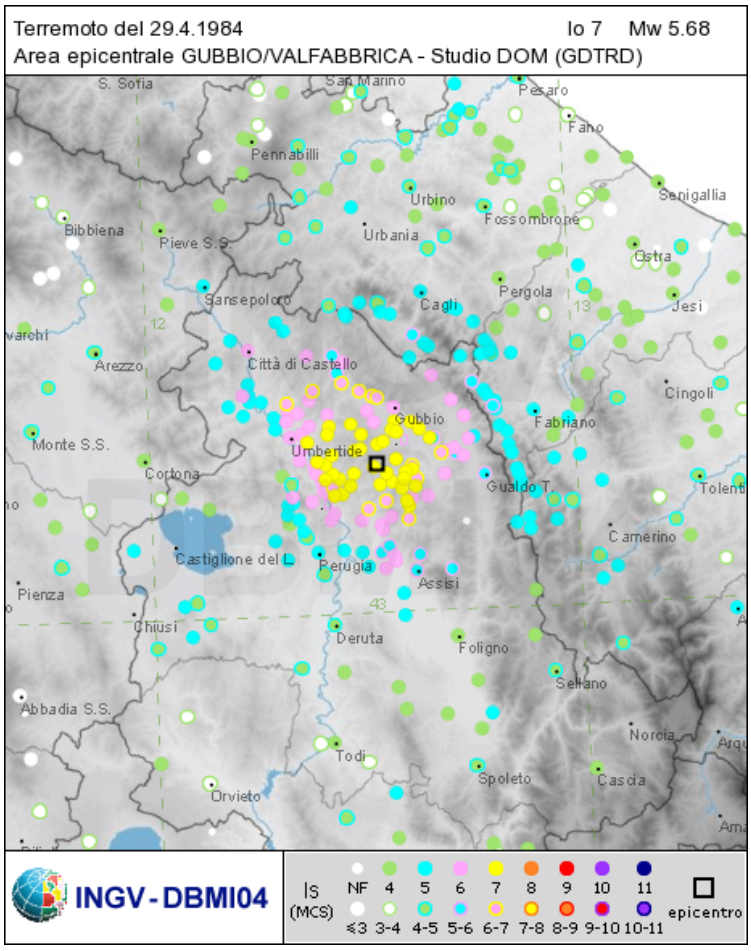

Figure 3.2.1 – Felt intensities for the 1984 Gubbio earthquake (From INGV-DBMI04;2007)

Five accelerometric stations belonging to the Rete Nazionale Accelerometrica, RAN, were triggered by the earthquake. Figure 3.2.2 shows the position of the stations with the recorded accelerograms. The maximum acceleration was recorded at Nocera Umbria station, located at about 20 km from the fault, but this station is strongly influenced by site effects with a maximum amplification around 6 Hz. (Castro et al.; 2004; Cultrera et al; 2003 and Figure 3.2.4).

All stations were equipped with analog instruments. The data were corrected for the instrumental response and filtered with a cosine bandpass filter. The high pass frequency was selected by visual inspection of the uncorrected Fourier spectrum. For all data, it was selected around 0.5 Hz, with the exception of UMB accelerograms filtered at 1 Hz, because of high noise level The low pass frequency was selected in

accordance to the natural frequency of the instrument (generally 25Hz).

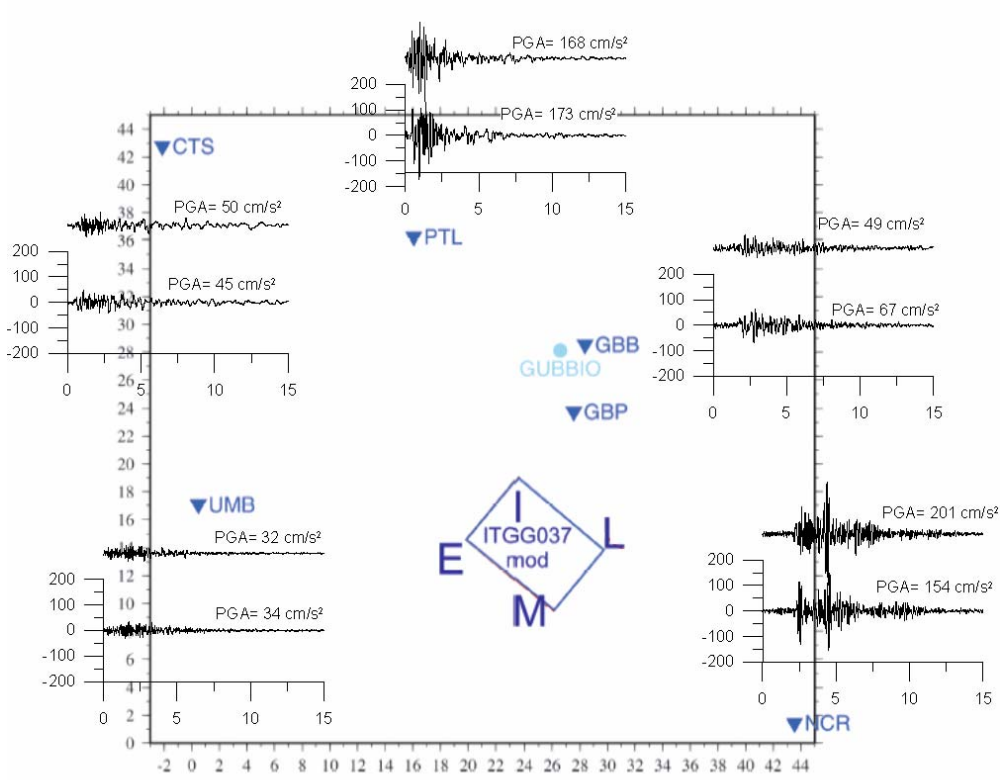

Figure 3.2.2 – Accelerometric stations triggered by the 1984 Gubbio earthquake. For each station, the two horizontal acceleration recordings are reported. The fault of the earthquake is indicated by the blue box.

The 1984 Gubbio earthquake was simulated using two hybrid techniques based on the extended fault and described in Deliverable D0-S3 (2006): deterministic-stochastic method, DSM (Pacor et al., 2005 and Progetto S3-Deliverable D0), and hybrid *k*-squared source modeling technique, HIC (Gallovic and Brokeshova, 2007 and Progetto S3 Deliverable D2).

To model the source and the propagation medium, we used the fault geometry and the crustal model described in the previous paragraph (Tables 2.2.1 and 3.1.1 and Figure 3.1.1).

No previous studies (such as waveform inversion analysis) were available to constrain "a priori" the position of the rupture nucleation point, the value of rupture velocity and final slip distribution on the fault. These parameters are necessary for a kinematic modeling of the earthquake source, so we decided to simulate several possible scenarios, varying rupture velocity and nucleation point, to define the best model to reproduce the 1984 earthquake wavefield. The adopted final slip model on the fault (Figure 3.2.3) is a k^{-2} slip distribution with a dominant asperity located in the central deeper section of the fault and has been considered as a fixed parameter of the model.

Since we want to define the best model only in terms of two kinematic parameters we decided to apply a simple grid search method rather than much complicated algorithm suitable for searching among several parameters.

The grid search has been performed by simulating 810 scenarios varying the hypocenter position and the rupture velocity over the fault. We investigated 90 nucleation points on the fault (equally spaced by 0.5 km), see figure 3.2.3, and 9 rupture velocities (from 0.6Vs to 1Vs, Vs=3.3 km/s).

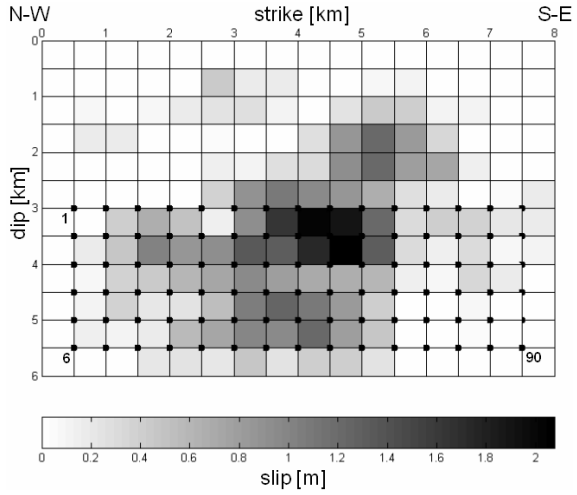

Figure 3.2.3 Fault geometry and final slip distribution adopted in the simulations. Black dots show the position and number of nucleation points used in the grid search.

The goodness-of-fit between synthetic and observed data was quantified in the frequency domain. For this purpose, we defined a misfit function:

$$\varepsilon = \frac{1}{m}\sum_{j=1}^{m} E_{rms}(f_j) \qquad (1)$$

where m is the number of the considered frequencies and being:

$$E_{rms}(f) = \left\{ \frac{1}{n}\sum_{i=1}^{n}\left[\log\left(\frac{SA(f)_{obs}}{SA(f)_{sim}} \right)_i \right]^2 \right\}^{1/2} \qquad (2)$$

where n is the number of stations and $SA(f)$ are the acceleration response spectra computed at selected frequencies.
Equation (1) and (2) are useful to define a unique number to quantify the goodness of the model computing residuals between observed and simulate response spectra ($\log_{10}(Sa_{obs})$-$\log_{10}(Sa_{sim})$). This formulation has been already used in several studies also considering the natural log of the spectral ordinates (Castro et al., 2005; Graves and Pitarka, 2004).

In order to minimize the influence of site effects, affecting some of the recorded data (Castro et al. 2004), we computed the previous equations in the frequency band 1-4 Hz, with the purpose of extending the results to a wider frequency range. This choice has been done considering that site effects are minimal in this frequency range. Nevertheless we have been forced to consider site amplification at NCR station since it is strongly affected by high frequency site effects between 3 and 9 Hz (see figure 3.2.4).

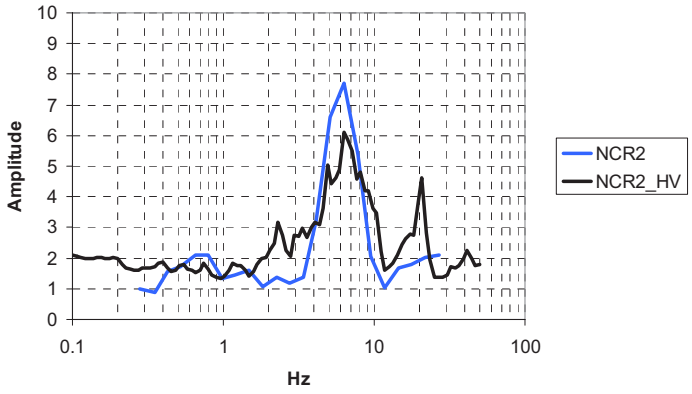

Figure 3.2.4 Horizontal to Vertical spectral ratio and empirical transfer function estimated by generalized inversion technique (Bindi et al; 2005) at NCR station

We also performed the grid search in the frequency band 0.5 – 2 Hz considering HIC method, which provide a reliable evaluation of the low-frequency content.

The results of grid search are shown in figure 3.3.5. Because of the trade-off between rupture velocity and nucleation point position, the minimum value alone of ε is not completely representative of the best model and another low value of ε could be obtained with different combination of nucleation point and rupture velocity. For this reason, we contoured, in the plots, scenarios giving a value of ε < 0.4 in order to represent the trend of ε function.

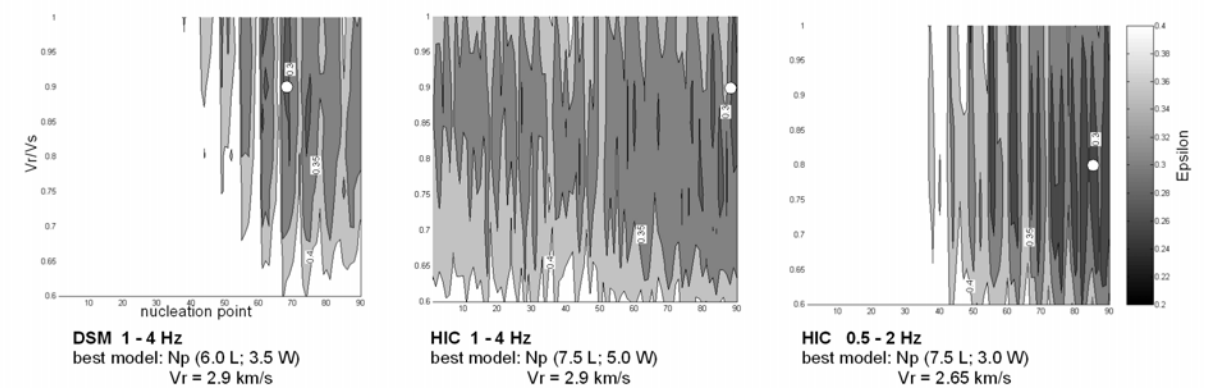

Figure 3.2.5 Grid search results. x-axis: number of the nucleation point, from 1 to 90 (see figure 3.2.3), y-axis: Vr/Vs values, from 0.6 to 1.

For both techniques (frequency band 1-4 Hz), the best model (minimum value of ε, white dots in figure 3.2.5) prefers high rupture velocity (0.9Vs) and a nucleation point located in the south-eastern side of the fault. In general, considering scenarios with model bias < 0.35, we can infer that a better fit with observed spectral values is obtained for relatively high rupture velocities (>0.75 Vs). However the choice of a particular *vr* doesn't seem to affect too much the model bias since values < 0.35 are obtained with a large range of possible rupture velocities.
In terms of position of rupture nucleation point the results obtained in grid search analysis are strictly related to the different approach in modeling the rupture

propagation on the fault adopted by the two techniques. The DSM method defines a deterministic envelope based on the isochron theory which makes the technique especially sensitive to the position of nucleation point. On the contrary in HIC method the high frequency source radiation is modeled by an incoherent sum of sub-sources. For this reason, looking at 1-4Hz frequency range an area of nucleation point corresponding to low ε values can be defined for the DSM result. On the other hand when we consider the HIC modeling we obtained low value of ε for a very large number of possible hypocenters. Nevertheless if we consider a lower frequency band (0.5-2 Hz) in the grid search, the coherent evaluation of the ground motion, in HIC method, at low frequency allows to identify an area of better-fitting nucleation point located, also in this case, in the S-E part of the fault.

The spectral acceleration residuals for the two best models (identified in the 1-4 Hz grid search), computed at different selected frequencies for each station and each horizontal component are shown in figure 3.2.6. Residuals computed respect to the spectral ordinates predicted by Ambraseys et al., 2005 ground motion prediction equation are also plotted (for maximum horizontal component and rock site). The low-frequency bias (f=0.5 Hz) has been computed only considering HIC simulations and removing station UMB that, because of the high level of noise, has been filtered below 1 Hz. The bias has been computed up to 9 Hz, since HIC synthetics have been low-pass filtered at 10 Hz. The general trend at frequencies ≤ 1Hz is over-estimation of the observed values. However, at PTL and CTC stations, the DSM model slightly under-predict observations. It is noteworthy that, at f=1 Hz, the model bias given by the two techniques is quite consistent; discrepancies are likely related to the surface waves recorded at CTC station (DSM simulates only direct s-waves) and to the influence of low-frequency radiation pattern (adopted in HIC modeling) at PTL station. The strong over-estimation at UMB, in both simulations, could still be related to the data processing.
AMB05 equation provide, in general, better results at f=0.5 Hz while the bias is quite similar with our models for f=1Hz. At this frequency the empirical model underestimates spectral ordinates for stations located in the forward directivity direction while overestimates the values at NCR (backward directivity). At these stations our models provide better residuals respect to the mean values predicted by AMB05. The better fit provided by the empirical values at f=0.5 Hz could be related, in our opinion, to the recorded data processing. Indeed, typically, accelerometric data are high-pass filtered with a f_{cut} around 0.5 Hz while HIC synthetics contain frequencies below 0.5 Hz. Furthermore the accelerometric data-set used by Ambraseys et al., 2005 has been likely processed with a similar filter. Therefore the over-estimation provided by HIC spectral ordinates and the better fit provided by AMB05 equation seem quite reasonable.

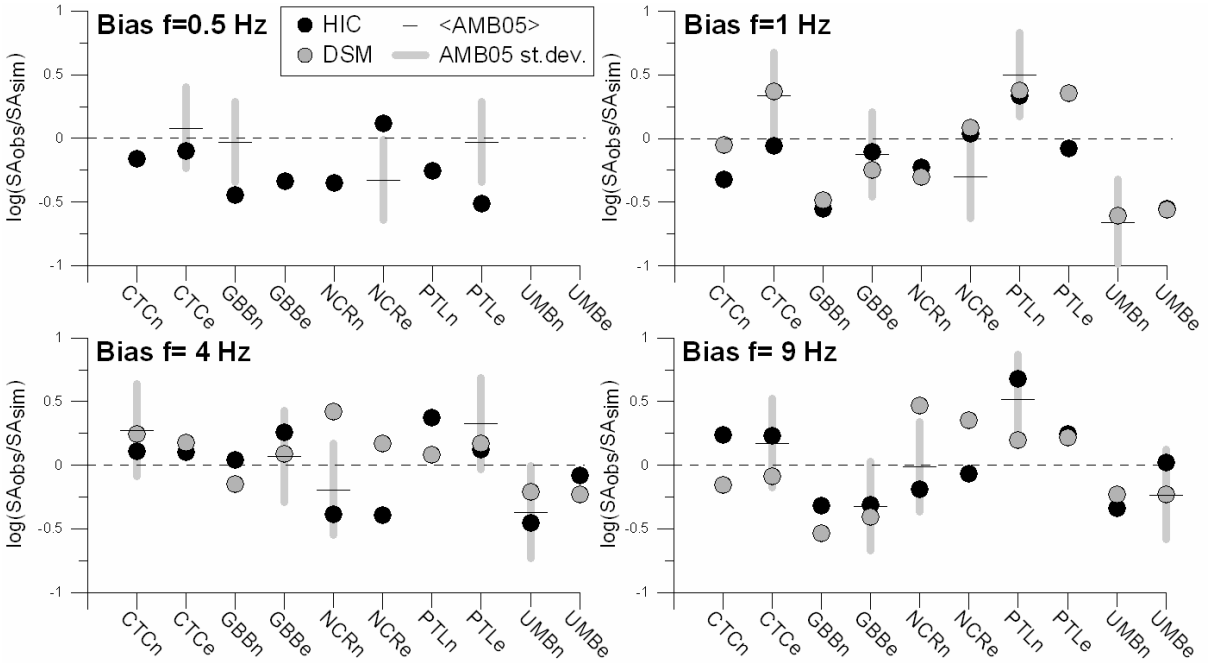

Figure 3.2.6 - Spectral acceleration model bias computed at selected frequencies. Black and gray dots represent model bias computed considering the HIC and DSM best model respectively (see figure 3.2.5). The model bias computed respect to Ambraseys et al.,2005 prediction equation is represented by black segments (for mean predicted values) and by gray bars for the one-standard deviation range.

At higher frequencies (f=4 and f=9 Hz) the difference in model bias between the methods increase for stations in the fault-strike direction (CTC, PTL and NCR). These stations are much sensitive to directivity effects and, as expected at high frequency, we obtained, with HIC technique, a negative model bias at NCR station and a positive one at PTL station. The same results are also given by AMB05 mean predicted values. DSM provide better results at PTL station where the high-frequency forward directivity is reproduced, nevertheless at NCR site (anti-directive) the synthetics underestimate the observed values up to a factor of 3.

If we average the residuals (showed in Figure 3.2.6) for all the stations and for both horizontal components at each frequency (3), we obtained the model bias plotted in Figure 3.2.7.

$$E(f) = \frac{1}{n}\sum_{i=1}^{n} \log\left(\frac{SA(f)_{obs}}{SA(f)_{sim}}\right)_i \qquad (3)$$

A model bias of zero indicates that sthe simulation, on average, matches the observed ground motion level. A negative model bias indicates over-prediction and a positive model bias indicates under-prediction of the observations.

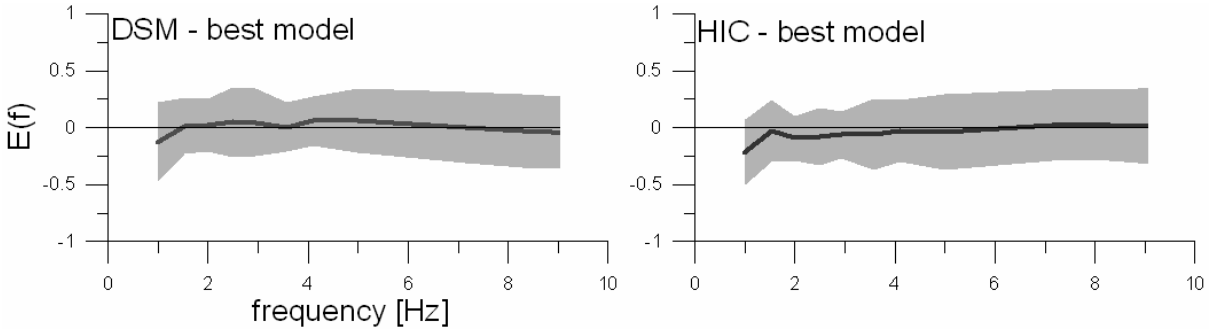

Figure 3.2.7 Spectral acceleration residuals averaged over 5 sites (equation 3). Thick line represents the mean model bias, shaded gray area represent the standard deviation of residuals distribution.

The simulation results have no significant bias over the frequency range 1 to 9 Hz, indicating that the simulation model adequately captures the main characteristics of the ground motion response. However an over-estimation trend is visible for the lower frequencies. The average standard error is about 0.3 for both simulation techniques.
Synthesizing we can argue that the most probable nucleation point of 1984 earthquake is located in a region of the fault included between 6.0 and 7.5 km along strike and 3.5 and 5.0 along dip (see Figure 3.2.3 and 3.2.5) producing a rupture propagation toward North with a rupture velocity likely around 2.9 km/s.
Both techniques provide consistent results and are able to reproduce reasonably well the spectral characteristics of the 1984 earthquake (Figure 3.2.7). However the two methodologies present peculiar features that make each technique appropriate for different aspects. DSM is able to reproduce phenomena related to the direction of rupture propagation such as directivity effects in the high frequency range. HIC is a much complete method suitable to capture features related to the low-frequency content (low-frequency directivity effects, radiation pattern, ground displacement) and to the subsequent seismic phases.
The modeling of 1984 earthquake allows to state some important results useful in the computation of shaking scenarios presented in section 3.3. 1) The adopted crustal structure and fault geometry represent a good approximation of the reality. 2) The adopted simulation techniques are able to produce realistic ground motion values and to model properly most of the observed near-field features better than ground motion prediction equations.

3.3 SHAKING SCENARIOS

The shaking scenarios studies for the Gubbio area have been performed considering the two fault geometries described in 3.1 section: ITGG037 fault and ITGG038 fault. The synthetic seismograms have been computed at 32 sites (Fig. 3.3.1), listed in Table 3.13 and 3.1.4.
The 27 sites inside the basin correspond to the locations of installed velocimetric stations and of performed noise measurements in this Project-Task6 (see PS3–Deliverables 22-23).

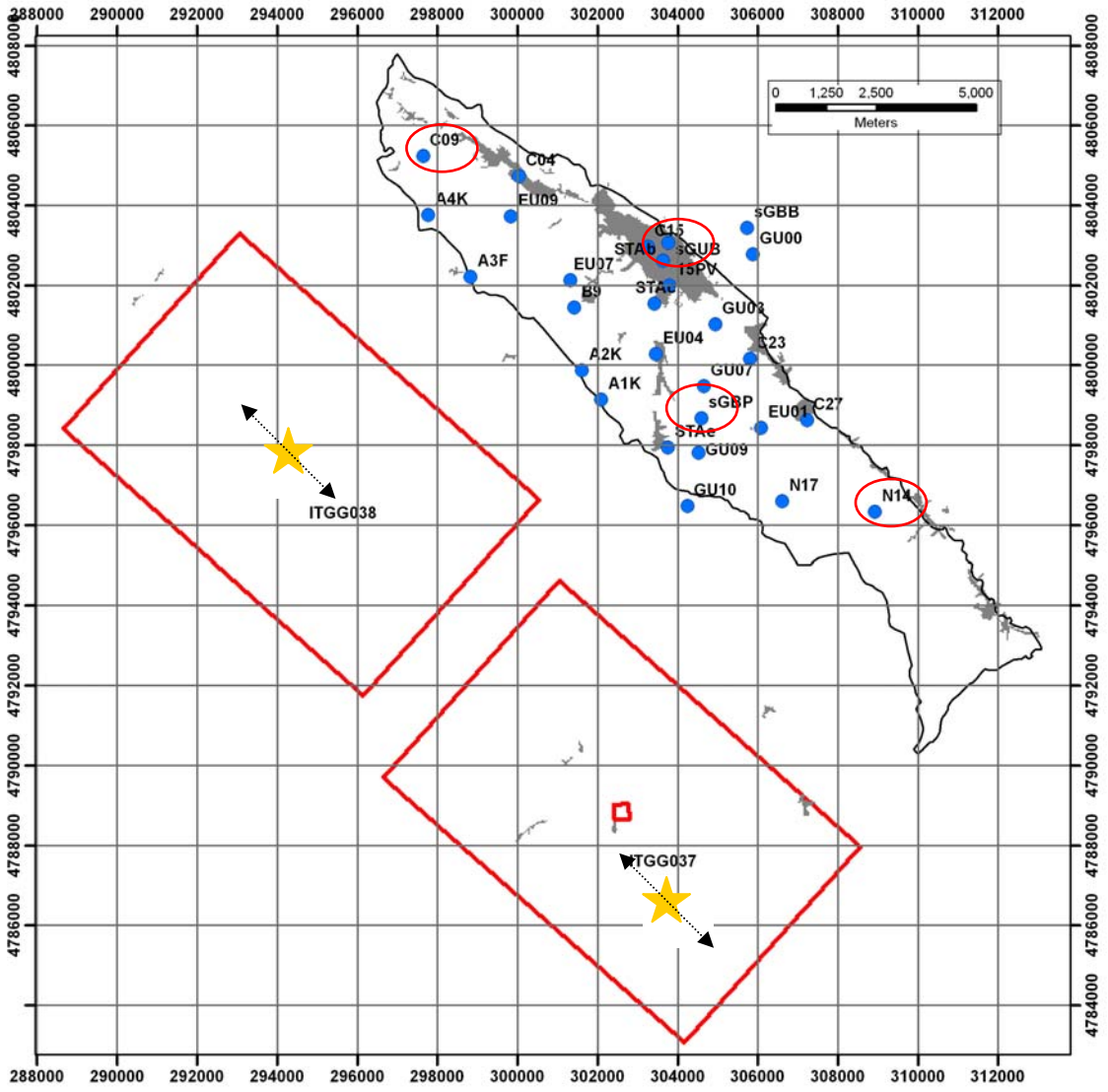

Fig 3.3.1 –Source models and site locations for the computation of shaking scenarios. The red circles indicate the four sites used for selecting representative shaking scenarios. The stars correspond to nucleation point generating mean shaking scenarios in the Gubbio basin.

The strategy for simulations counts different level of complexity (PS3-Deliverable D1).
At level 0 we computed simple scenarios by applying the UMA05 ground motion prediction equation (Bindi et al.; 2005) in the Gubbio basin area. This equation provides peak values (PGA and PGV) as a function of hypocentral distance and site condition and it is based on a data-set strictly related to the Gubbio region (mainly from the 1997-1998 Umbria-Marche seismic sequence). Nevertheless it only accounts for average characteristics of ground motion, and Near-Fault effects cannot be captured by this model. Furthermore synthetic seismograms representative of the maximum credible earthquake cannot be predicted.

The shaking scenarios at level 1 are simulated by DSM modelling technique (PS3-Deliverables D0 and D1).
We simulated more than 8200 scenarios for both fault geometries varying the three

main kinematic parameters describing the rupture models: position of nucleation point, value of rupture velocity and final slip distribution on the fault.
In particular we investigated 152 nucleation points located in the deeper half of each fault, 9 rupture velocities (from $0.6V_s$ to $1V_s$) and 6 different k^{-2} slip distribution (figure 3.3.2).
This extensive number of simulations has been performed at only 4 sites within Gubbio basin: GBP, Gubbio city (GUB), C09 and N14. The locations of these sites have been chosen in order to represent roughly the basin's geometry.

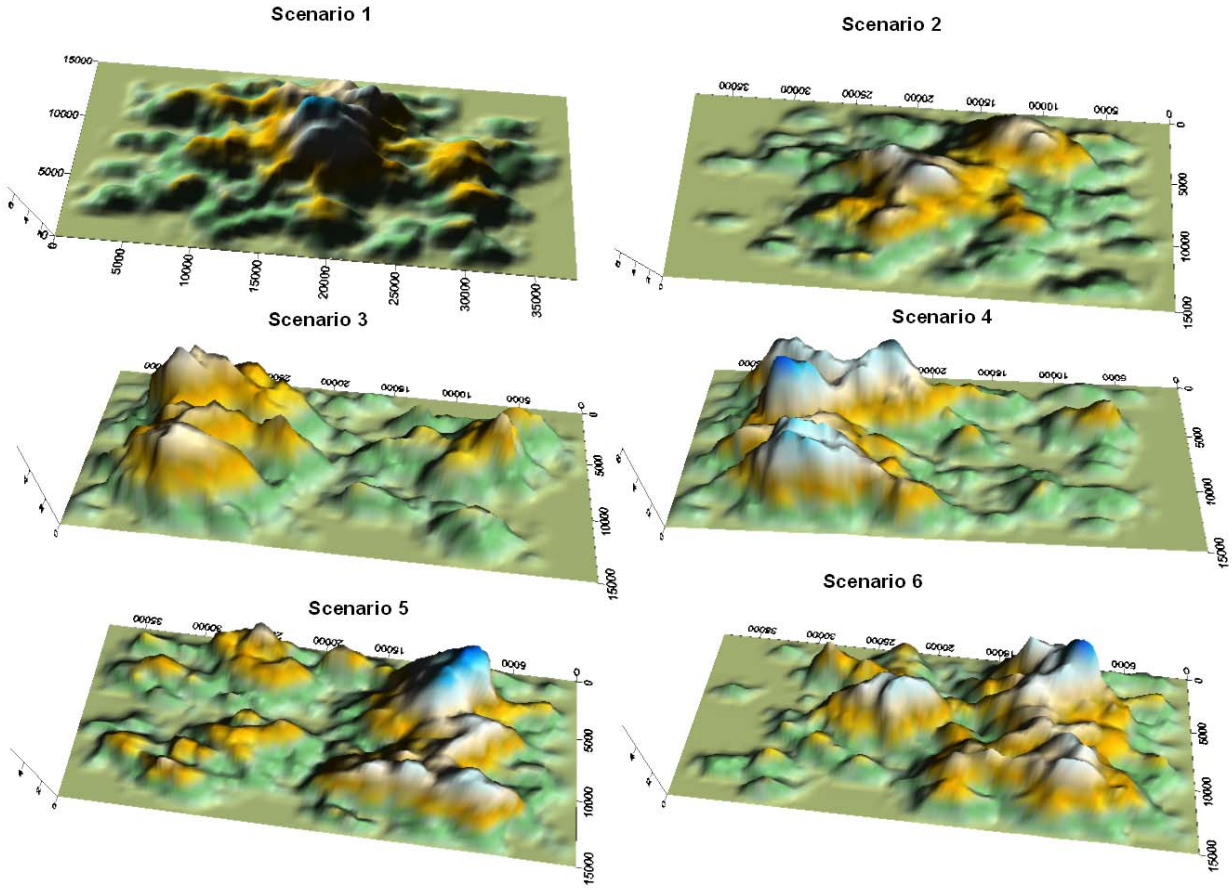

Figure 3.3.2 - Slip distributions used to generate shaking scenarios in the Gubbio area.

The purpose of generating this huge number of scenarios is to obtain, at the 4 sites, a distribution of ground motion parameters representative, as much as possible, of all the shaking values that could be expected in the area if one of the faults would activate. Figure 3.3.3 shows the PGA synthetic distribution obtained for sites N14 and GBP, simulating the rupture scenarios on the fault ITG038.

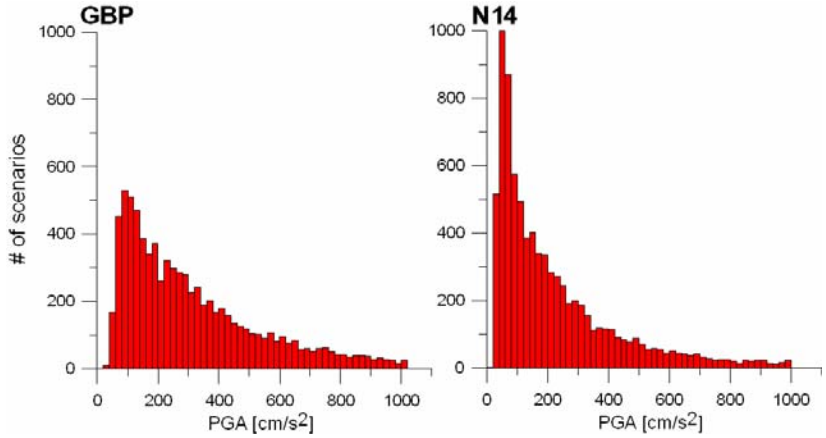

Figure 3.3.3 - Shaking scenarios at level 1 for ITGG038. Peak ground acceleration distribution at site GBP and site N14, obtained simulating 8200 different rupture scenarios. Y-axis represents number of scenario in each PGA bin. The synthetic data follow a log-normal distribution.

Figure 3.3.4 shows the PGA distribution at each site as a function of distance compared with UMA05 prediction equation. Black bars represent the range of PGA values obtained at each site for all the 8200 scenarios. Black dots represent the mean value of each distribution and red bars the range of 1 standard deviation. Gray shaded area is the UMA05 ±σ predicted values at each distance.
It can be noticed that the mean values and the associated standard deviation of synthetic distributions are quiet consistent with the empirically predicted values.

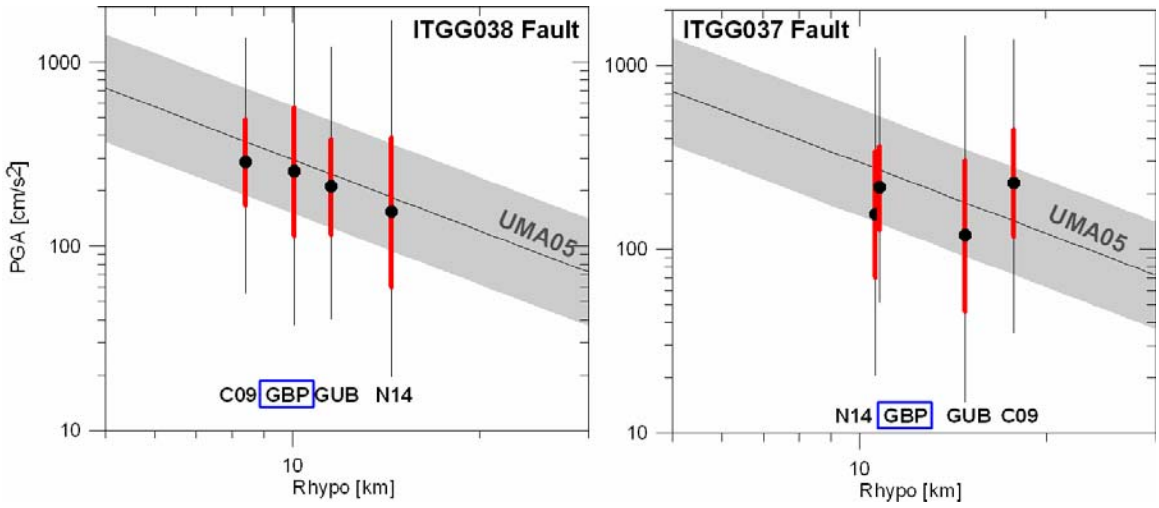

Figure 3.3.4 - Shaking scenarios at level 0 and level 1 for ITGG038 (Left) and ITGG037 (Right).

In order to provide time series associated to the rupture of the two sources, we need to select a single scenario occurring on the faults.
To do this, we focused on GBP accelerometric station, located in the centre of the basin, to identify the rupture scenario producing the peak ground acceleration (PGA) closest to the mean value of the distributions. Once defined this "mean" scenario we computed time series at all the 27 sites located in the Gubbio basin and at Gubbio city.

In this way, time series has been calculated only for scenario providing mean PGA value at GBP station. Note that in the selection of the "mean" scenario we also took into account the mean values produced at the other 3 stations, used as check points. The shaking scenarios giving mean values are defined by the following parameters:

- ITGG038 fault: Slip model #4
  Rupture velocity = 2.9 km/s
  Nucleation point = 5 km strike / 3.5 km dip

- ITGG037 fault: Slip model #4
  Rupture velocity = 2.65 km/s
  Nucleation point = 7 km strike / 4.5 km dip

The two scenarios correspond to a bilateral and quasi-unilateral rupture toward N-W, respectively. For the two faults, the mean PGAs inside the basin are 0.28g and 0.33g gal. At Gubbio city, the PGAs are 0.27g. These values are very close to the ones proposed by the Italian seismic hazard map (MPS04; Gruppo di Lavoro MPS (2004). 2004) for the return period of 475 years.

The horizontal synthetic acceleregroms simulated at GBP site are shown in Figure 3.3.5

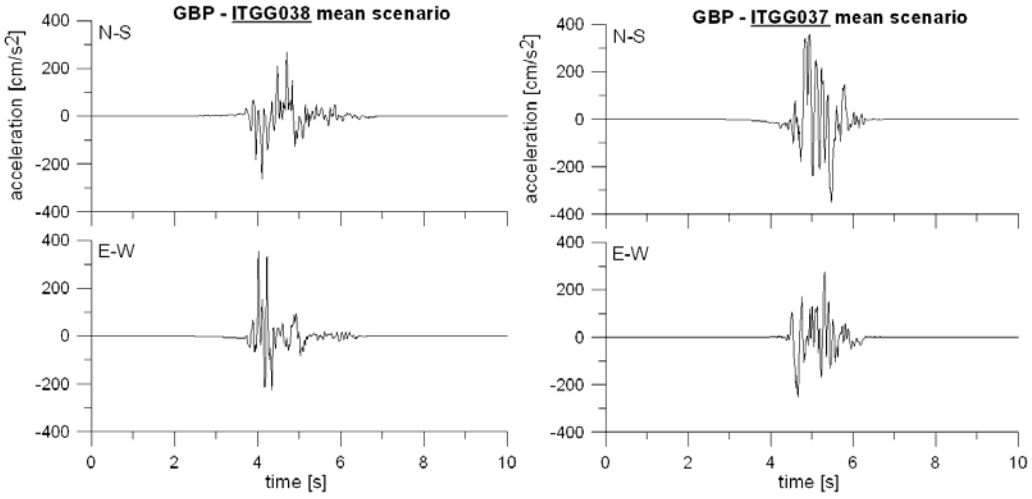

Figure 3.3.5 - Shaking scenarios at level 1: synthetic accelerograms computed at GBP station for the rupture scenarios giving mean PGA at the four selected sites. Left: fault ITGG038; Right: fault ITGG037; Up: NS component; Down: WE component

In Figure 3.3.6, horizontal spectral acceleration SA (5% damping) for the four check sites are plotted, compared with the Eurocode spectrum, scaled at the mean values of synthetic PGA at the four sites and equal to 0.25g, for class soil A.

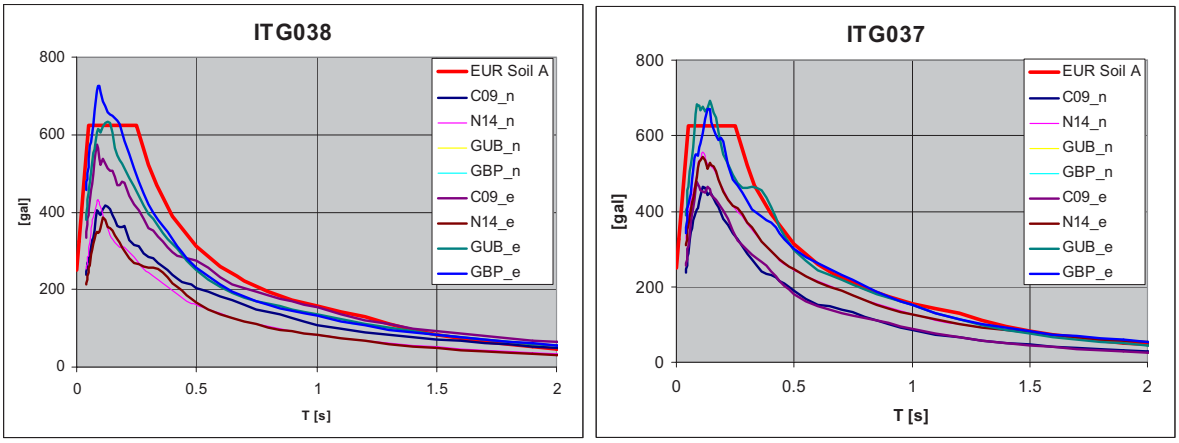

Figure 3.3.6 - Shaking scenarios at level 1 for ITGG038 (Left) and ITGG037 (Right). Comparison between acceleration response spectra and Eurocode spectra scaled at 0.25g for class soil A.

Finally in Figures 3.3.7a and b the PGA and SA at T = 1s maps are shown.

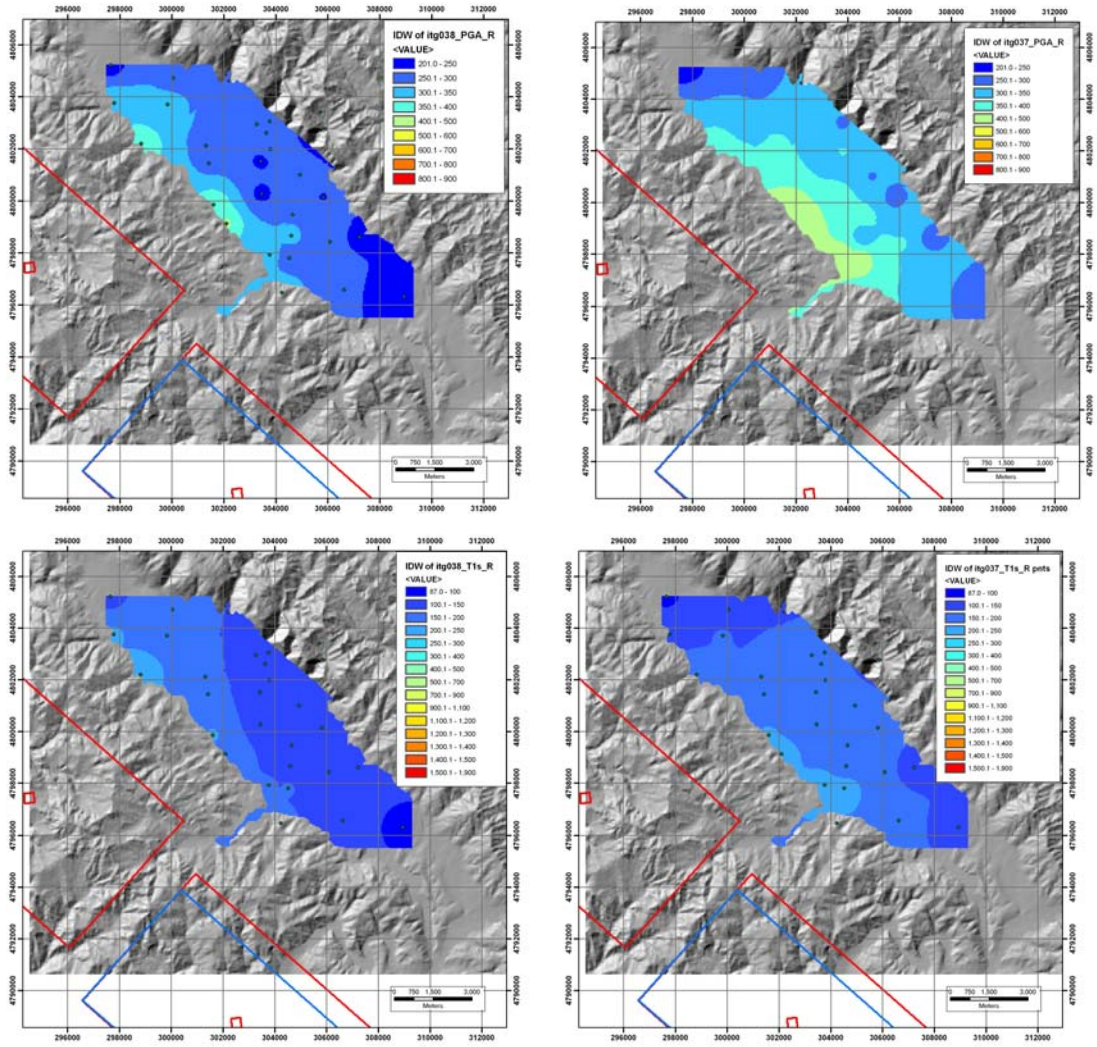

Figure 3.3.7 - Shaking scenarios at level 1 for ITGG038 (Left) and ITGG037 (Right). Top: PGA maps. Bottom Spectral acceleration at T = 1s.

The two faults generate shaking scenarios very similar. The higher PGA values are found for the fault ITG037 with the maximum on the south-west border of the basin; the spectral accelerations at 1s have a very uniform distribution with the maximum located in the zone of the basin nearest to the seismogenic fault.

Starting from these selected scenarios, we perform the level 2 of the ground motion prediction in the Gubbio area.
The shaking scenarios at level 2 were performed computing broad band synthetics, in order to provide time series containing the complete wave-field at low frequency (< 1 Hz). In this study, the low frequency component of the ground motion up to 2.5 Hz was simulated using the COMPSYN technique, described in Deliverable D0 and D1.
The broad band signals are obtained through the combination, in the frequency domain, of deterministic COMPSYN low-frequency waveforms with stochastic DSM high-frequency synthetics. This approach yields strong motion seismograms that cover the whole frequency range of engineering interest (0 – 20 Hz). We reconcile the amplitude spectra of seismograms calculated by the two techniques at intermediate frequencies where their domain of validity overlaps. The frequencies f_a and f_b *identify* the transition band where the low and high frequency seismograms are combined: for frequency f < fa the contribution to the broad band signal is completely given from the low frequency part; at frequency f > fb, the broad band signal is equal to the high frequency seismogram. In the transition band the two signals are weighted as that the sum is equal to unity at each frequency. The broad-band strong motion signal contains exact low frequency near-field terms and approximate high frequency contributions. The intermediate frequency band, where the high and low frequency seismograms were merged, was selected by visual analysis, identifying the overlapping frequency range. In average, the transition band is from 1.3 – 1.5 Hz. For each site, we verified that the near field terms, not included in the DSM simulation, were preserved.
In Figures 3.4.8 and Figure 3.4.9 we present examples of broad band signals for the sites C09 and GBP, generated from the fault ITG038. We note the spectral content at frequency less than 1.5Hz are very similar and no special features related to low frequency phenomena as high permanent displacement or directivity pulse are present for the selected scenarios. Similar results are also found for the ITG037 fault.

In this case the use of shaking scenarios computed at level 1 provide a good description of the ground motion expected at Gubbio city and at the Gubbio basin. For this reason, the following analysis including site effects and described in PS3 Deliverables D22-D23, will be performed using synthetic seismograms generated al levels 1.

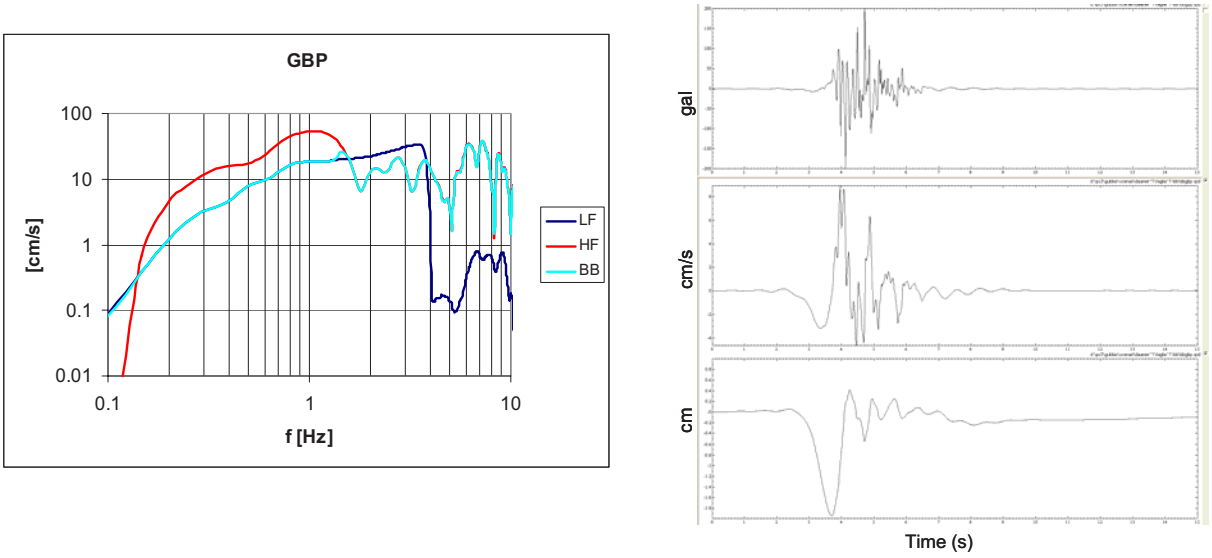

Figure 3.4.8 – a) NS component of amplitude Fourier spectra of low frequency LF, high frequency HF and composite signals BB for site GBP and fault ITG038 fa and fb are 1.3Hz and 1.5Hz, respectively **b)** Broad band acceleration, velocity and displacement seismograms for site GBP and fault ITG038.

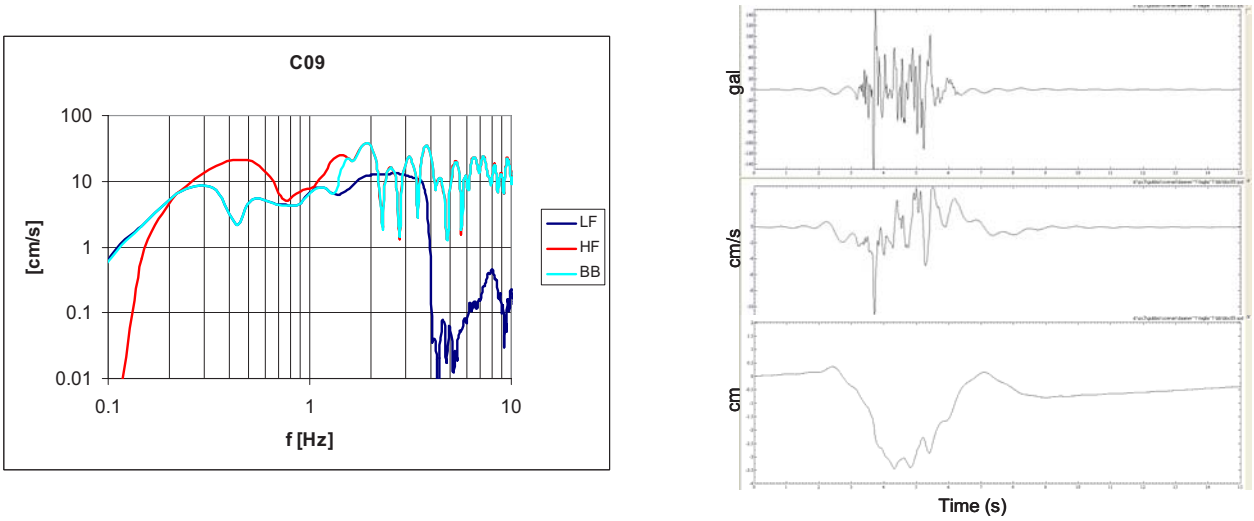

Figure 3.4.9 – a) NS component of amplitude Fourier spectra of low frequency LF, high frequency HF and composite signals BB for site C09 and fault ITG038 fa and fb are 1.3Hz and 1.5Hz, respectively **b)** Broad band acceleration, velocity and displacement seismograms for site C09and fault ITG038.

3.4. PROBABILISTIC DETERMINISTIC SHACKING SCENARIOS

The result of probabilistic seismic hazard analyses (PSHA) consist of hazard maps or curves representing the values of a selected strong ground motion parameter having a fixed probability of exceedance for a given period of time. Due to the integral nature of the PSHA, each point on the curve combines the effect of all seismic sources both in terms of magnitude, geometry and rate of occurrence that can affect a site of interest.
The selection of the most appropriate strong ground motion parameter depends on the target of the analysis. From an engineering point of view, the most frequently used parameters are the peak ground acceleration (PGA), peak ground velocity (PGV) or response spectra (Sa) for different values of the structural period.
However, the most complete result of a PSHA is represented by the Uniform Hazard Spectra (UHS). In fact, UHS is an envelope of the spectra from a suite of earthquakes and provides a multi-parametric description of ground motion and is made up of spectral ordinates values that have an equal likelihood of being exceeded. It differs from a deterministic response spectrum in so far as, the response spectrum values at each period are largely independent of each other (Reiter, 1990).
From a practical point of view, an UHS for a given site is obtained by calculating a suite of hazard curves, one for each selected structural period and then, for the selected probability of exceedance or frequency of exceedance, by retrieving the corresponding ground motion value.
In particular, if A indicates a selected strong ground motion parameter, the computation of the hazard curve, requires the solution of the classical hazard integral (Cornell, 1968) that, for the i-th selected seismic source zones and a range of possible magnitudes and distances, is given by:

$$E_i(A \geq A_0) = \alpha_i \int_R \int_M f_R(r) f_M(m) p_a\left[A(m,r) \geq A_0 | m,r\right] dm\, dr \qquad (1)$$

In equation (1), the conditional probability of exceedance p_a that, for a given distance r and a given magnitude m, allows to compute the probability of exceedance of a threshold value A_o depends on the selected empirical attenuation model. The expression of the probability density functions $f_M(m)$ and $f_R(r)$ depends respectively upon the adopted earthquake recurrence model (e.g., Gutenberg-Richter) and upon the source geometry that can be a point, a line or a bounded surface. On the other hand α_i , for each seismic zone, represents the average rate of occurrence of the earthquakes in a fixed range of magnitude.
Starting from equation (1), that represents the frequency of exceedance, by selecting a time of interest t which depends on the life-time of the selected structure, assuming a Poissonian distribution for the event $A \geq A_o$ it is possible to calculate the probability of exceedance in the following form:

$$P(A \geq A_0, t) = 1 - e^{-E_i(A \geq A_o)t} \qquad (2)$$

Thus, once the set of structural period of interest has been selected, for each period the hazard integral in equation 1 is solved and for the fixed probability of exceedance the value of A is retrieved to form the final UHS. Figure 3.4.1 shows a schematic

example of UHS calculation for a selected 50% of probability of exceedance and 11 structural periods.

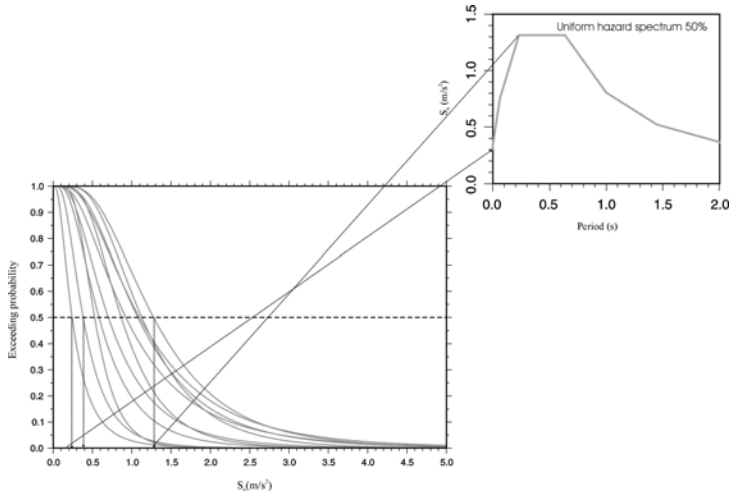

Figure 3.4.1 – Left panel: Exceeding probability curves for a synthetic test and 11 selected structural periods. Upper panel: UHRS for a 50% of probability of exceedance.

All the previous considerations apply when the modified version of the classical hazard integral is used in the framework of the probabilistic-deterministic approach (PDHA) aimed at calculating the hazard for a single fault. Detailed theoretical aspects of the PDHA are described in the deliverable D2.
In the following section the PDHA is used to calculate the UHS for two faults and three site located in the Gubbio area.

3.4.1 Application to Gubbio area

In the present project the probabilistic-deterministic approach for a characteristic earthquake scenario proposed by Convertito *et al.* (2006) has been applied to perform hazard analysis considering two faults and three sites of interest in the Gubbio area. Site location, fault characteristics and magnitude are reported in the paragraph 3.1 of the present deliverable.
In order to calculate the hazard curves and the UHSs, for each of two faults, that is, ITGG037 and ITGG038, and three sites GBB, GCT and GCC, the PDHA has been applied by using the spectral acceleration as strong ground motion parameter and assuming that this parameter is governed by a log-normal distribution. The analysis has been performed by selecting 11 structural periods T= 0.0, 0.1, 0.15, 0.20, 0.30, 0.40, 0.50, 0.75, 1.00, 1.50 and 2.0 s and four return periods that is, T_r= 20,000, 30,000, 40,000 and 50,000 years. The selection of the return periods is based on the computed activity rate for the two faults by using the approach of Schwarz and Coppersmith (1984) and by ensuring the occurrence of at least one earthquake occurrence. Given the fault parameters configuration and the magnitude value (M 6.0) for which the analysis have to be performed the activity rate for the two faults and the characteristic part of the earthquake recurrence model was 6.62 10^{-4} $years^{-1}$. This means that, for the shortest considered return period (T_r=20,000 years) about 13 earthquakes occur. The parameters used to retrieve the characteristic earthquake

recurrence model valid for both faults are listed in Table 3.4.1.
For each scenario, the values of the strong ground parameter for the north-south (NS) and east-west (EW) component both in terms of median values and standard deviations have been calculated by using the simulation technique HIC proposed by Gallovic *et al.* (2007) described in details in the deliverable D2. The number of different rupture processes simulated was 864 for the ITGG037 fault and 432 for the ITGG038 fault.

Table 3.4.1 – Characteristic earthquake recurrence model parameters used to calculate the activity rate for the two faults ITGG037 and ITGG038.

***b*-value of the zone 919**	-1.22
M_{min}	4.2
Mean slip-rate	0.05 cm/year
M_{min} (scenario)	5.37
M_{max} (scenario)	6.37
Δm_1	1.0
Δm_2	1.0

For comparison, the same parameters for the 11 selected structural periods, have been calculated by using the empirical model proposed by Sabetta and Pugliese (1996). This allows to enlighten the differences between a classical PSHA analysis and PDHA analysis when applied at a single fault.

3.4.2 Results for the site GBB

The results for the GBB site relative to the two faults and two components of the ground motion are reported in Figure 3.4.2, 3.4.3, 3.4.4 and 3.4.5 respectively. In each figure, the lower panel refers to UHS obtained when the simulated data are used while the upper panel refers to the case in which the empirical attenuation model proposed by Sabetta and Pugliese (1996) is used. Each red and blue line refers to a given return period. Due to the assumed log-normal distribution of ground motion parameter, the results obtained computing the integral in equation (1) cause that the larger is the return period the larger are the response spectra values. The selected structural periods are identified by the circles.
Black line in each panel represents the values of Sa corresponding to the minimum state of knowledge, that is, when only magnitude and location of the event are known. Figures 3.4.2a and b show the results obtained for the two components and the fault ITGG037 while Figures 3.4.3a and b refer to the fault ITGG038. The differences in the results may be ascribed to the differences in the median and dispersion values, when synthetic or empirical data are used. On the other hand, the differences between the results referring to the two components NS and EW for each single fault are ascribed to the adopted simulation technique and are not present in the results obtained by using the Sabetta and Pugliese (1996) empirical model. This is due to the fact that the empirical models provide strong ground motion estimates only for the largest horizontal component and do not account for the source characteristics such as focal mechanism, slip distribution on the fault plane and directivity and geometrical effects.

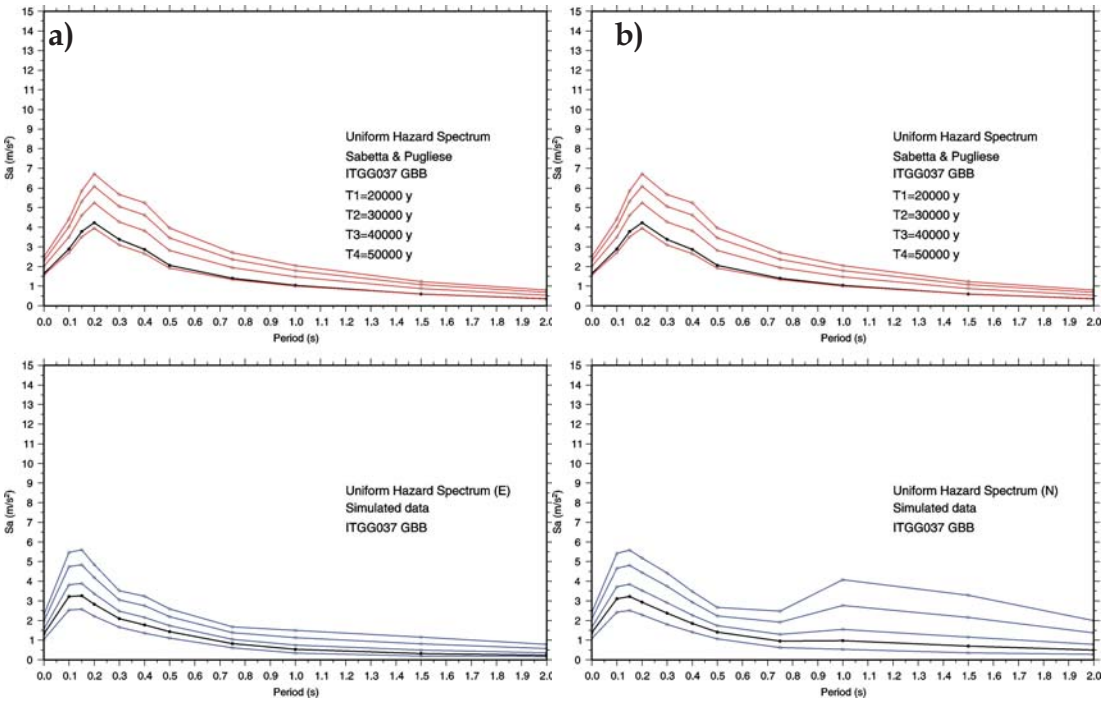

Figure 3.4.2 – Lower panel: UHS in terms of pseudo relative acceleration for the GBB site computed by using simulated data and the fault ITGG037. Each curve corresponds to a selected return period. The black line represents the median spectrum computed for each structural period (see text). Upper panel: UHS for the same fault and site pair computed by using the empirical attenuation model proposed by Sabetta and Pugliese (1996). **a)** EW component **b)** NS component .

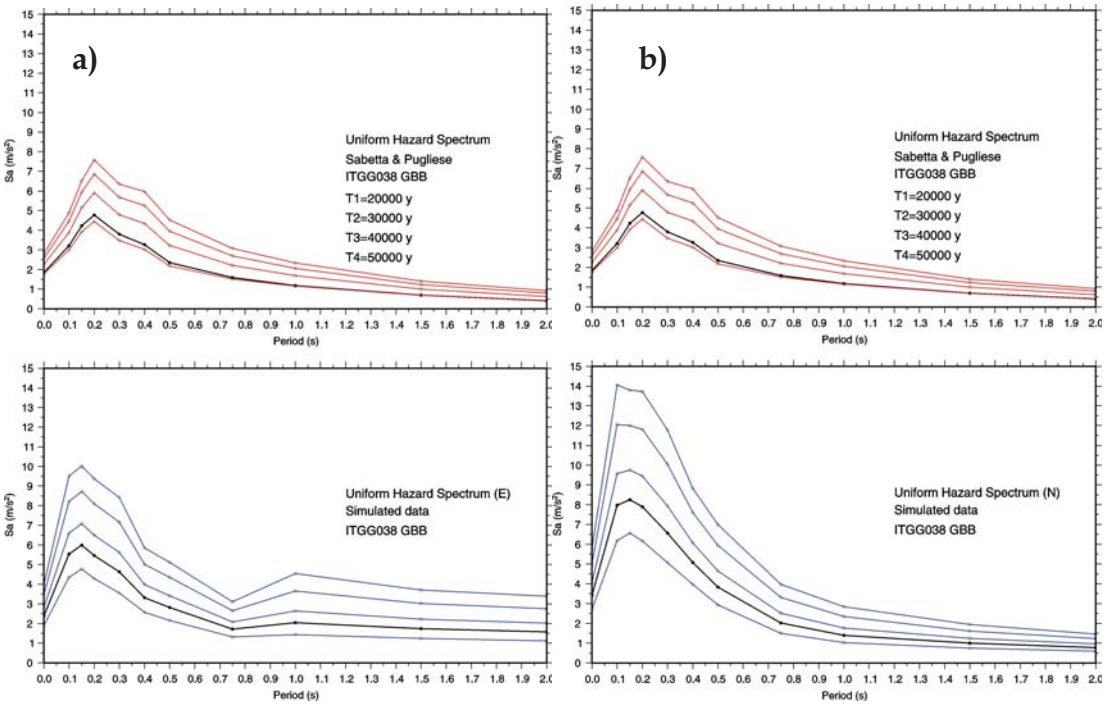

Figure 3.4.3 – Lower panel: UHS in terms of pseudo relative acceleration for the GBB site computed by using simulated data and the fault ITGG038. Each curve correspond to a selected return period. The black line represents the median spectrum computed for each structural period (see text). Upper panel: UHS for the same fault and site pair computed by using the empirical attenuation model proposed by Sabetta and Pugliese (1996). **a)** EW component **b)** NS component .

For comparison in Figure 3.4.4 are shown the UHSs retrieved from the Italian national hazard map (Meletti, 2006) for the same structural periods and two values of the probability of exceedance. In particular, the 10% and 2% of probabilities of exceedance in 50 years have been selected. The first probability is the classical probability value corresponding to a return period T_r = 475 years. The latter value, that is 2%, corresponds to the smaller available probability value in the hazard map and a return period T_r = 2,475 years. This value has been chosen because in the PSHA approach, for a given time of interest and a fixed seismic source geometry, the smaller is the selected probability the larger is the probability of occurrence of large earthquakes thus providing conditions similar to those used to apply the PDHA.
The comparison allows to enlighten the differences between the classical approach for the hazard computation where all the earthquakes in a fixed magnitude range can occur in the seismic source zone and the result obtained when the PDHA is applied considering a single earthquake on a given fault as scenario.

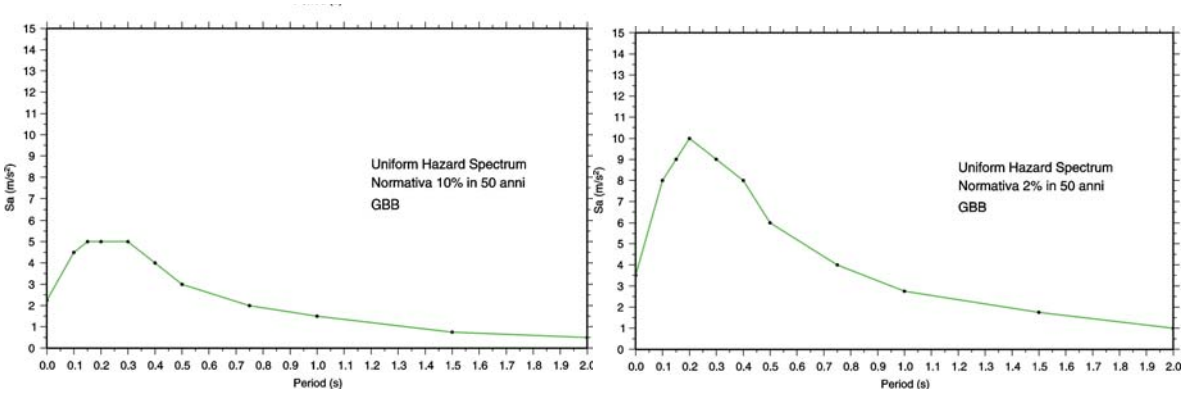

Figure 3.4.4 – UHS retrieved from the Italian hazard map. Left panel refers to the UHS computed for site GBB, the same structural periods and a 50% probability of exceedance in 50 years. Right panel refers to the same site but to a 2% probability of exceedance in 50 years.

3.4.3 Results for the site GCT

Figures 3.4.5a and b and 3.4.6a and b show the UHSs for the same two faults and the site GCT. Again lower panels refer to the UHSs calculated by using simulated data and upper panels to empirical data.
Due to the source-to-site distance, the results are different when the two faults are taken into account. The shorter is the distance the larger are the Sa values. The first difference concerns the values of the spectral ordinates when simulated data are taken into account with respect to those obtained by using the Sabetta and Pugliese (1996) empirical attenuation model. In fact, empirical data provide UHSs quite similar for the two faults and for each selected return period. On the other hand, when simulated data are used, the highest Sa values correspond to the NS component and the fault ITGG038 that is at a shorter distance with respect to the fault ITGG037. However, looking at the dispersion of the curves for both the NS and EW components and the two faults note that the shape of the UHSs are quite regular except for the EW component relative to the fault ITGG038 and the NS component relative to the fault ITGG037 particularly for larger structural periods. The differences may be ascribed to the location of the site with respect to the focal mechanism and to the slip variability on the fault plane. In particular, the smaller frequencies, that 1.0 and 1.5 s, have larger dispersions in the simulated data.

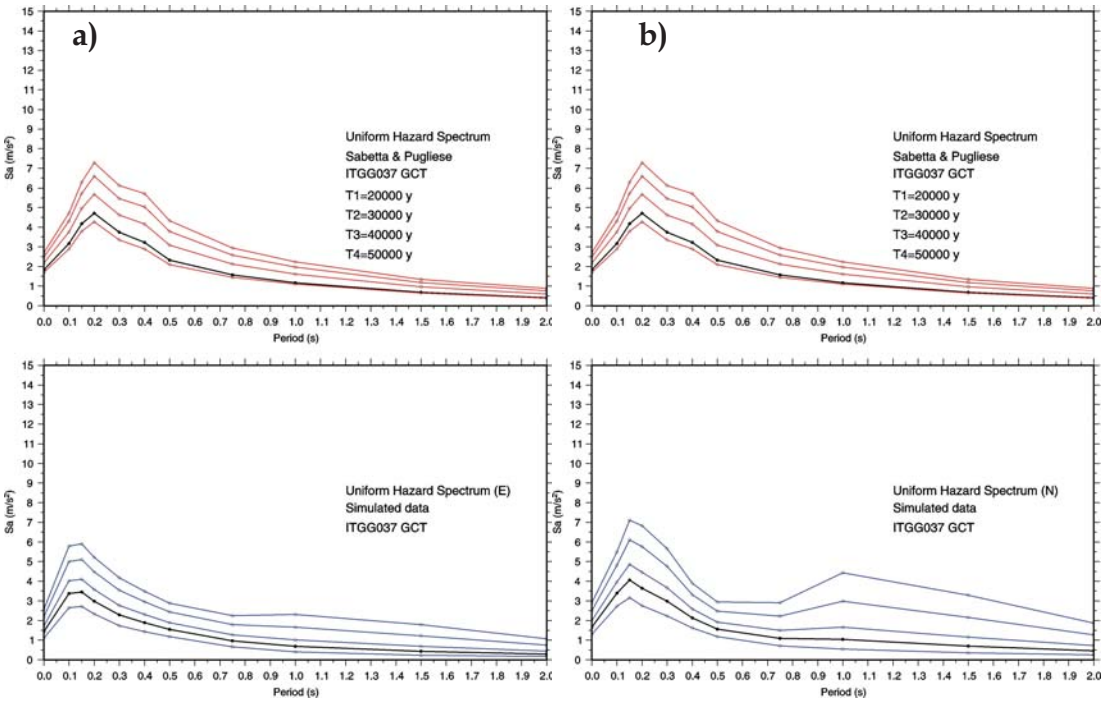

Figure 3.4.5 – Lower panel: UHS in terms of pseudo relative acceleration for the GCT site computed by using simulated data and the fault ITGG037. Each curve correspond to a selected return period. The black line represents the median spectrum computed for each structural period (see text). Upper panel: UHS for the same fault and site pair computed by using the empirical attenuation model proposed by Sabetta and Pugliese (1996). **a)** EW component **b)** NS component .

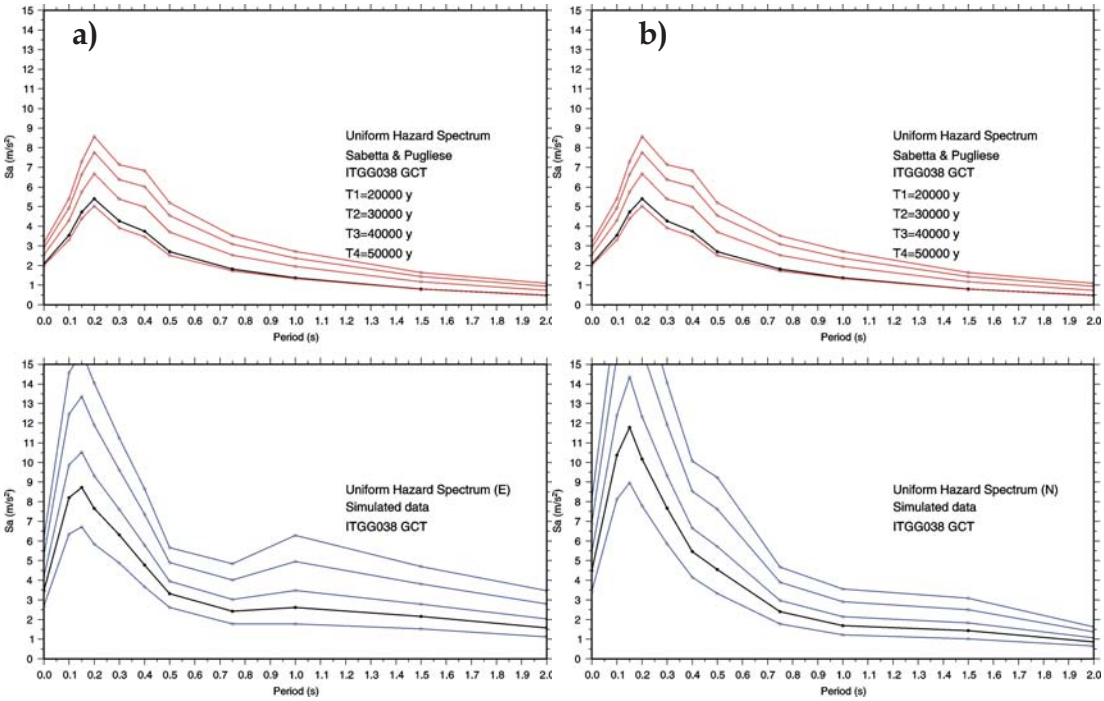

Figure 3.4.6 – Lower panel: UHS in terms of pseudo relative acceleration for the GCT site computed by using simulated data and the fault ITGG038. Each curve correspond to a selected return period. The black line represents the median spectrum computed for each structural period (see text). Upper panel: UHS for the same fault and site pair computed by using the empirical attenuation model proposed by Sabetta and Pugliese (1996). **a)** EW component **b)** NS component .

3.4.4 Results for the site GBP

The site GBP is the nearest between the three sites at both the two faults and, as a consequence, the largest values of spectral ordinates are expected. These considerations are confirmed looking at the Figures 3.4.7a and b, and 3.4.8a and b, that show the results for the two faults and the two data. When the Sabetta and Pugliese (1996) empirical attenuation model is taken into account the UHSs are quite similar due to similar source-to-site distance from the two faults. On the other hand, when the results relative to simulated data are taken into account very different results are obtained. In particular, the differences between the two faults and the two components may be firstly ascribed to the different dispersion values associated at each structural period. The differences in the dispersion values are due to both site location with respect to the focal mechanisms and the up-dip directivity effect that affect the two components differently. However, for the same fault the differences in the values of the spectral ordinates for different periods, such as those relative to the NS component and ITGG037 fault, can be also ascribed to the slip distribution that affect different frequencies in different way.

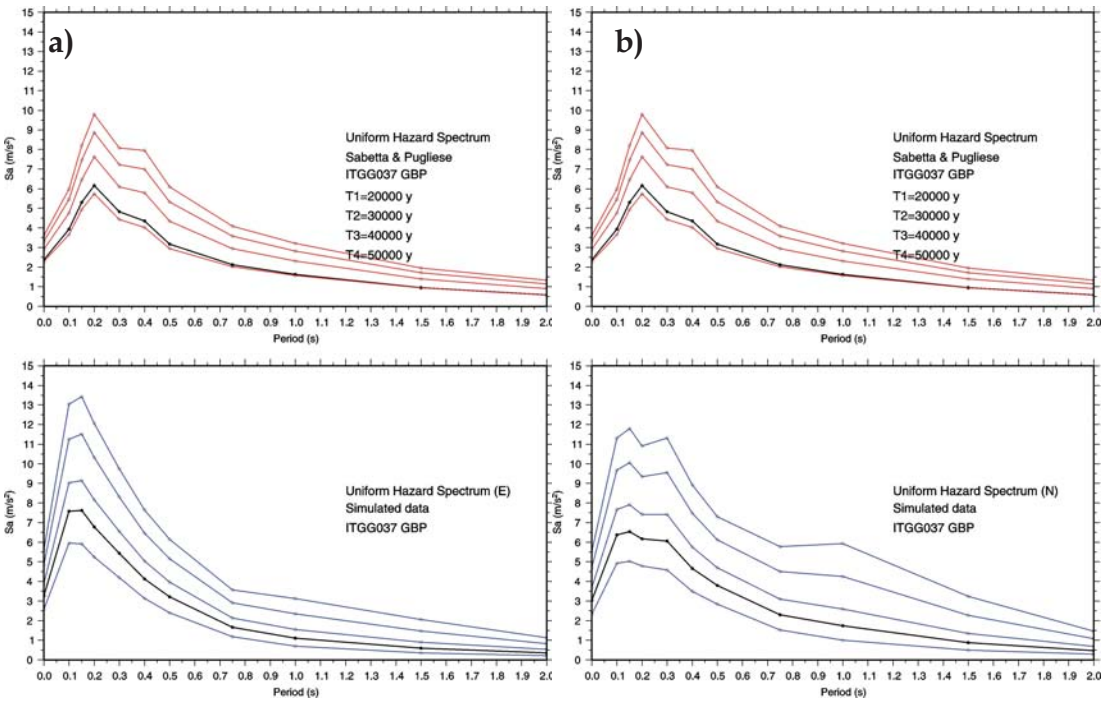

Figure 3.4.7 – Lower panel: UHS in terms of pseudo relative acceleration for the GBP site computed by using simulated data and the fault ITGG038. Each curve correspond to a selected return period. The black line represents the median spectrum computed for each structural period (see text). Upper panel: UHS for the same fault and site pair computed by using the empirical attenuation model proposed by Sabetta and Pugliese (1996). **a)** EW component **b)** NS component .

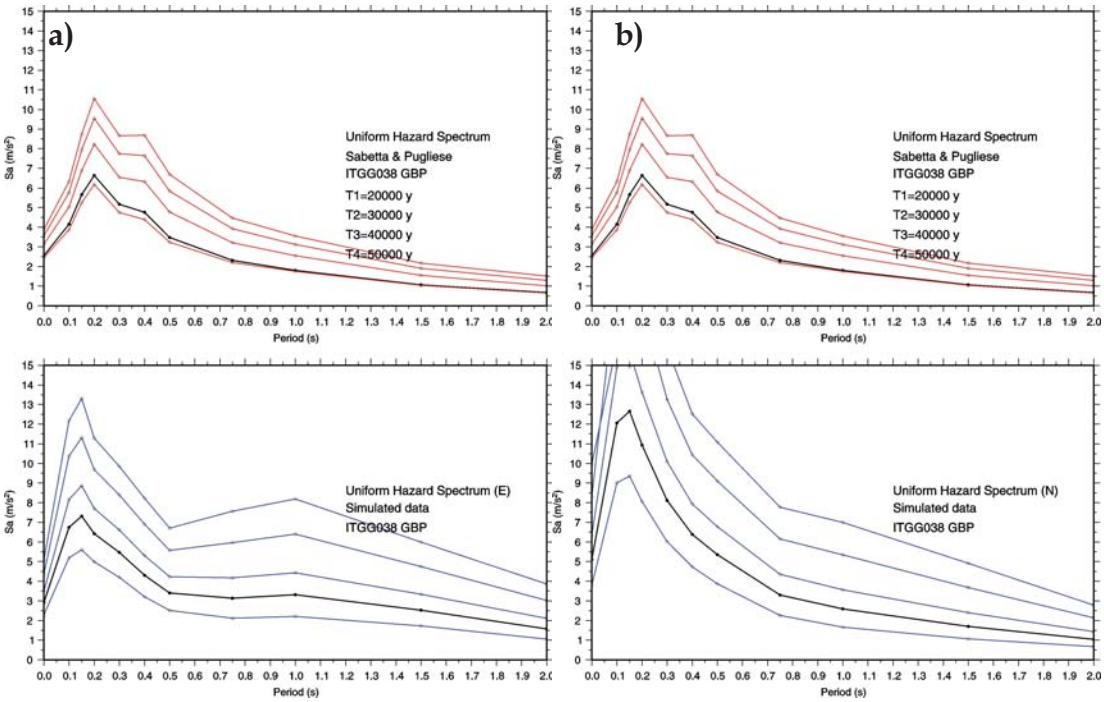

Figure 3.4.8 – Lower panel: UHS in terms of pseudo relative acceleration for the GBP site computed by using simulated data and the fault ITGG038. Each curve correspond to a selected return period. The black line represents the median spectrum computed for each structural period (see text). Upper panel: UHS for the same fault and site pair computed by using the empirical attenuation model proposed by Sabetta and Pugliese (1996). **a)** EW component **b)** NS component.

4. DISCUSSION AND CONCLUSION

All the performed analyses for the Gubbio area could be taken as example of what should be done as the information available change and/or increase.
The classical Probabilistic Seismic Hazard Analysis (PSHA approach) could be the starting point for evaluating shaking scenarios for one or more sites. The only necessary information is: the seismic zones of interest (and, obviously, their characteristics in terms of geometry and seismic activity) and a good empirical ground motion model. In this study we skipped this part because we have richer information and we focus our attention on the Deterministic Hazard Seismic Analysis (DHSA approach).
After having defined the reference earthquakes and individuated the seismogenic faults, the deterministic scenarios can be computed considering several rupture processes, everyone possible from the physical point of view, developing on the faults. For each rupture process, synthetic seismograms are simulated at the sites of interest and, due to the large number of seismograms available, the ground motion parameters can be estimated trough a statistical analysis. Furthermore when real data are available, preliminary study can be performed in order to get some insight about the source kinematic parameters and the propagation medium. Finally if information about the recurrence characteristic of the significant fault are available, the results from the deterministic scenarios can be integrated in the frame of the probabilistic approach in order to obtain a "dynamic" scenario, where the time variable in introduced in the deterministic case and the deterministic aspects of the

source rupture in the frame of the probabilistic approach.
In the Gubbio area, two major sources (ITGG037, ITGG038), were identified as capable to generate earthquakes of M = 6. A part of the fault to the south (ITGG037) is thought to be the source of the 1984 Gubbio earthquake (M 5.7).
Using the accelerometric data recorded during this event a detailed modelling study was performed in order to verify the simulation capability of the DSM and HIC techniques. Through a grid search procedure applied in a narrow frequency band (1-4Hz and 0.5 - 2Hz) we found the rupture scenario of the 1984 Gubbio earthquake was characterized by a rupture propagation toward North with a rupture velocity likely around 2.9 km/s. Both technique provide consistent results and reproduce reasonably well the spectral characteristics of the observed data.
The modeling of 1984 earthquake make us confident about crustal structure and fault geometries to be adopted in the following generation of predictive shaking scenarios. Furthermore the results show that the simulation techniques are able to produce realistic ground motion values and to model properly most of the observed near-source features better than ground motion prediction equations.

The predictive bedrock scenarios were computed at level 0 and level 1. The ground motion at level 2 was computed in order to verify the approximation degree introduced by the shaking scenarios generated at level 1.
To evaluate the effects of the rupture of the extend faults we select four site representative of the Gubbio city and the Gubbio basin and simulate more than 8200 kinematic scenarios for each fault varying the rupture velocity, slip distribution and nucleation point for each source using the DSM technique.
The synthetic PGAs distributions were compared with those predicted by the empirical models. The results show that the mean values and the associated standard deviation of synthetic distributions obtained by level 1 are quiet consistent with the empirically predicted values (level 0).
Finally in order to provide synthetic time series to be used for evaluating shaking scenarios including site effects, the rupture model giving the mean values was selected. The synthetic seismograms at levels 2 generated from these shaking scenarios have frequency content very similar to those computed at level 1, indicating that non special effects at low frequency as directivity pulses and high permanent displacements should be expected in the Gubbio area.

We found the average PGA values inside the basin PGAs are 0.28g and 0.33g gal for ITGG038 and ITGG037, respectively. For both sources at Gubbio city (GUB), the PGAs are 0.27g, very close to the ones proposed by the Italian seismic hazard map for the return period of 475 years.

REFERENCE

Ambraseys, N.N., Douglas, J., Sarma, S.K., Smit, P.M. (2005) Equations for the estimation of strong ground motions from shallow crustal earthquakes using data from Europe and Middle East: Horizontal peak ground acceleration and spectral acceleration, Bull. of Earthquake Engineering, 3, 1-53.

Barba, S., and R. Basili (2000). Analysis of seismological and geological observations for moderate-size earthquakes: the Colfiorito Fault System (Central Apennines, Italy). Geophys. J. Int., 141, 241-252.

Barchi, M., M. Cardinali, P. Chiraz, C. Collettini, C. Federico, F. Guzzetti, M. B. Magnani, G. Minelli, F. Mirabella, C. Pauselli, G. Pialli, S. Pucci and E. Troiani (2000). Integrazione di dati geofisici e geologici per la caratterizzazione delle strutture sismogenetiche di Colfiorito e di Gubbio. F. Galadini, C. Meletti and A. Rebez (eds), Le ricerche del GNDT nel campo della pericolosità sismica (1996-1999), CNR-Gruppo Nazionale per la Difesa dai Terremoti-Roma, 149-156.

Basili, R., G. Valensise, P. Vannoli, P. Burrato, U. Fracassi, S. Mariano, M.M. Tiberti, E. Boschi (2007). The Database of Individual Seismogenic Sources (DISS), version 3: summarizing 20 years of research on Italy's earthquake geology. Tectonophysics (submitted).

Bindi D., Luzi L., Pacor F., Franceschina G. and Castro R.R. (2006). Ground-motion predictions from empirical attenuation relationships versus recorded data: the case of the 1997-1998 Umbria-Marche, Central Italy, strong-motion data set, Bull. Seismol. Soc. Amer., 96, 3, 984-1002.

Boncio, P., F. Brozzetti and G. Lavecchia (2000). Architecture and seismotectonics of a regional low-angle normal fault zone in Central Italy. Tectonics, 19, 1038-1055.

Castro, R. R. and E. Ruı´z-Cruz (2005) Stochastic Modeling of the 30 September 1999 Mw 7.5 Earthquake, Oaxaca, Mexico. Bull. Seism. Soc. Am. 95, No. 6, 2259-2271.

Castro, R. R., Pacor, F., Bindi, D., Franceschina, G and L. Luzi (2004) Site Response of Strong Motion Stations in the Umbria, Central Italy, Region. Bull. Seism. Soc. Am. 94, No. 2, 576-590.

Castro, R., F. Pacor, D. Bindi, G. Franceschina, and L. Luzi (2004). Site response of strong motion stations in the Umbria, Central Italy, Region. Bull. Seism. Soc Am. 94, 576-590.

Ciaccio, M.G., M.R., Barchi, C. Chiarabba, F. Mirabella, E. Stucchi, 2005. Seismological, geological and geophysical constraints for the Gualdo Tadino fault, Umbria–Marche Apennines (central Italy). Tectonophysics, 406, 233-247

Convertito V., A. Emolo, and A. Zollo (2006). Seismic-hazard assessment for a characteristic earthquake scenario: an integrated probabilistic-deterministic method, Bull. Seism. Soc. Am. 96, 377-391, doi:10.1785/0120050024.

Cornell, C. A. (1968). Engineering seismic risk analysis, Bull. Seism. Soc. Am. 58, 1583-1606.

CPTI Working Group, 2004. Catalogo Parametrico dei Terremoti Italiani, version 2004 (CPTI04). INGV, Milan, available from http://emidius.mi.ingv.it/CPTI/.

Cultrera G., Rovelli A., Mele G., Azzara R., Caserta A. and Marra F. (2003). AzimuthdependentAmplification of Weak and Strong Ground Motions within a Fault Zone (Nocera Umbra,Central Italy), J. Geophys. Res. 108 (B3), 2156, doi:10.1029/2002JB001929.

De Martini, P. M., N.A. Pino, G. Valensise and S. Mazza (2003). Geodetic and seismologic evidence for slip variability along a blind normal fault in the Umbria-Marche 1997-1998 earthquakes (central Italy). Geophys. J. Int., 155, 819-829.

DISS Working Group (2006). Database of Individual Seismogenic Sources (DISS), Version 3.0.2: A compilation of potential sources for earthquakes larger than M 5.5 in Italy and surrounding areas. http://www.ingv.it/DISS/, © INGV 2005, 2006 - Istituto Nazionale di Geofisica e Vulcanologia - All rights reserved.

Gallovic, F. and J. Brokesova (2007). Hybrid k-squared source model for strong ground motion simulations: introduction. Physics of the Earth Planetary Interior, 160, 34-50.

Gallovič, F. and J., Brokešová (2007) Hybrid k-squared Source Model for Strong Ground Motion Simulations: Introduction. Phys. Earth Planet. Interiors 160, 34-50,

Graves, R. and A. Pitarka (2004). Broadband time history simulation using a hybrid approach. 13th World Conference on Earthquake Engineering, Vancouver, British Columbia, 1–6 August 2004.

Gruppo di Lavoro MPS (2004). Redazione della mappa di pericolosità sismica prevista dall'Ordinanza PCM 3274 del 20 marzo 2003. Rapporto Conclusivo per il Dipartimento della Protezione Civile, INGV, Milano-Roma, aprile 2004, 65 pp. + 5 appendici.

Mai, P. M., Spudich, P. and J. Boatwright (2005) Hypocenter Locations in Finite-Source Rupture Models. Bull. Seism. Soc. Am. 95, No. 3, 965-980.

Meletti, C. (2006). Convenzione INGV-DPC 2004 – 2006. Progetto S1. Proseguimento della assistenza al DPC per il completamento e la gestione della mappa di pericolosità sismica prevista dall'Ordinanza PCM 3274 e progettazione di ulteriori sviluppi. URL: http://esse1.mi.ingv.it/

Pacor, F., Cultrera, G., Mendez, A. and M.Cocco (2005) Finite Fault Modeling of Strong Ground Motions Using a Hybrid Deterministic–Stochastic Approach. Bull. Seism. Soc. Am. 95, No. 1, 225-240.

PS3-Deliverable D0 (2006). Task1 – Scenari di Scuotimento - Deliverable D1 - Tecniche di simulazione, Giugno 2006

PS3-Deliverable D1 (2007). Task1 – Scenari di Scuotimento – Deliverable D1 - Linee Guida per il calcolo degli scenari di scuotimento, Luglio 2007

PS3-Deliverable D2 (2007). Task1 - Scenari di Scuotimento - Deliverable D2 - Innovative approaches to predict seismic ground motion, July 2007

PS3-Deliverable D21 (2007). Task6 – GUBBIO - Deliverable D21 - Geological model of the Gubbio Basin (Italy) for the characterisation of local seismic response, July 2007

PS3-Deliverables D22-D23 (2007). Task6 – GUBBIO - Deliverables D22-D23 - Shaking scenarios including site effects, July 2007

Pucci, S., P. M. De Martini, D. Pantosti and G. Valensise (2003). Geomorphology of the Gubbio Basin (Central Italy): understanding the active tectonics and earthquake potential. Ann. Geophys.-Italy, 46, 5, 837-864.

Reiter, L. (1990). Earthquake Hazard Analysis. Columbia University Press, New York, 254 pp.

Sabetta F., and A. Pugliese (1996). Estimation of response spectra and simulation of nonstationarity earthquake ground motion. Bull. of the Seismic. Soc. Am. 86, 337-352.

Schwartz, D. P., and J. Coppersmith (1984). Fault behaviour and characteristic earthquakes: examples from Wasatch and San Andreas faults, J. Geophys. Res. 89, 5681-5698.